ORIGINAL ARTICLE



- Investigation of the mechanical and hygrothermal behavior of coffee
- ground wastes valorized as a building material: analysis of mix designs
- 4 performance and sorption curve linearization effect
- ⁶ Stéphanie Gascoin²
- ⁷ Received: 7 April 2022 / Revised: 5 November 2022 / Accepted: 26 November 2022
- 8 © Wroclaw University of Science and Technology 2022

9 Abstract

10

12

13

14

15

16

17

18

19

20

24

25

26

27

28

29

30

31

32

33

Coffee ground wastes (CGW) are by-products from the coffee-making processes. In this study, we propose to valorize them in construction materials at large scale. In particular, we investigate the mechanical and hygrothermal performances of earthen cob construction with incorporation of various amounts of CGW. Our results indicate that adding coffee grounds to cob enhances its hygrothermal performances as well as its compressive strength. An interesting enhancement of the lightened earth thermal characteristics as well as a good control of the hydric load in the air while maintaining acceptable mechanical properties is observed. Numerical analysis is used to evaluate the hygrothermal behavior of cob specimens to better understand their energy performances. A simplification of the simulation methods using a linearization of the sorption curve is incorporated to reduce calculation times and optimize outputs. The method is validated using experimental data, which shows a promising improvement compared to previous approaches. The proposed method can be faithfully applied to the study of hygrothermal behavior of biomaterials, which is strongly related to the building energy performance and the investigation of their durability in a fast and efficient way.

- ²¹ **Keywords** Bio-based building materials · Mechanical/hygrothermal behavior · Linearized sorption curve ·
- ²² Numerical simulation · Hysteresis effect

23 1 Introduction

Earthen building has been existing for several ten thousand years in North-Africa and the Middle East, and numerous old earthen structures remain present today [1]. Earthen construction refers to the use of earth as a primary building material. It may be seen as a stand-alone natural construction concept or as a collection of techniques that ensure higher hygrothermal, durability, and environmental sustainability to more standard contemporary construction methods [2]. Communities and people all around the globe are using earth

building to limit their impacts to greenhouse gas emissions and global warming [3]. Typical earth-building methods that employ soil as a construction material include adobe or mud brick, rammed earth, cob, poured earth, and pressed earth [4]. Cob is the most traditional earth-building technique in Normandy (France) and Britany, which incorporates earth, sand, water, and fibers [5]. Cob is a traditional building method that employs hand-formed earthen clods combined with sand and fibers such as straw and reed. Fibrous materials, such as reed, are commonly utilized to prevent autogenous shrinkage in earth materials and give the optimum thermal performance. Several investigations have found that lightened earth mixtures have a great potential to interact with moisture. Earth-straw and earth-hemp combinations are among the insulating materials with the greatest degree of water buffering value and a good capacity of a material to manage the humidity of a space.

The structural behavior of cob buildings can be influenced by a variety of environmental conditions. Increased water content (due to rising humidity or a leaking roof)



34

35

36

37

38

39

40

41

42

43

44

45

46

47

48

49

50

A1 ⋈ Yassine El Mendili A2 yassine.elmendili@esitc-caen.fr

A3 Laboratoire ESITC Caen - COMUE Normandie Université, A4 1 Rue Pierre Et Marie Curie, 14610 Epron, France

A5 ² CRISMAT, UMR CNRS N°6508, ENSICAEN, IUT
A6 Caen, Normandie Université, 6 Boulevard Maréchal Juin,
14050 Caen, France

54

55 56

57

58

59

60

61

62

63

65

66

67

68

69

70 71

72

73

74

75

76

77

78

79

80

81

82

83

84

85

86

87

88

89

90

91

92

93

94

95

96

97

98

99

100

101

102

103

104

weakens the mechanical properties of the material and lead to the swelling of the fibers. Voids or micro-cracks can be generated at the fiber-matrix interface [6]. Due to the high fiber content, insects and rats can tunnel deep into cob walls [6]. All of these factors wreak havoc on cob walls' overall structural integrity. Furthermore, clay soil used traditionally for cob building has differential settlements, weak shear strength, and high compressibility [6], all of which must be stabilized to optimize mechanical performance [5]. Stabilization by chemicals or minerals is a new method for this purpose [2]. To stabilize clayey soil, cementitious binders such as portland cement, fly ash, and silica fume can be used. When these binders are applied to the soil-water or soil-fiber-water complex, they trigger a series of short and long-term chemical reactions that promote soil element flocculation, resulting in significant increases in composite stiffness and shear strength [7]. Despite their efficiency in terms of stability, cementitious binders are widely recognized as not being environmentally friendly. Significant energy and carbon emission footprints are usually worsened with their use [8]. According to literature, synthetic or natural polymers, resins, and sulfonated oils are promising replacement materials capable of meeting both geotechnical and sustainability requirements [9]. Polymers, like traditional cementitious binders, can facilitate the flocculation and hydration of clay particles via a variety of clay-polymer interaction mechanisms, such as (a) van der Waals or hydrogen bonding, (b) charge neutralization (via electrostatic attraction), and (c) cationic bridging for neutral, cationic, and anionic polymers [10].

Among the currently available polymer-based soil stabilizers, biopolymers, which are made from natural resources, appear to offer a variety of intriguing soil physical properties, outperforming synthetic counterparts in terms of sustainability [11]. Lignin is a biopolymer that is found in the highest concentration of plants biomass [12]. The enzymatic dehydrogenation of coumaryl, coniferyl, and sinapyl alcohols and subsequent radical polymerization produce this biopolymer with a great structural diversity. Hardness, resistance to microbial assaults, and oxidative stress are all aspects of this heterostructure, which makes biodegradation more difficult. One of the not exploited sources of lignin is coffee ground wastes (CGW) [13], an abundant and often discarded household and industrial waste, a potentially rich source of products and energy. The physicochemical properties of CGW enable its re-use in a variety of applications, as a biorefinery feedstock due to the presence of useful chemical compounds, as a raw material in the production of activated carbon or as a biosorbent in pollutant removal from gas or liquid due to its surface characteristics [13]. Implementing ecologically friendly methods based on coffee waste requires a greater understanding of its physicochemical features [13]. These latter usually depend on plant species, soils and growing conditions and subsequent preparations.

105

106

107

108

109

110

111

112

113

114

115

116

117

118

119

120

121

122

123

124

125

126

127

128

129

130

131

132

133

134

135

136

137

138

139

140

141

142

143

144

145

146

147

148

149

150

151

152

153

154

155

156

157

Coffee has become the second most traded commodity in the world after oil, and the second most popular liquid after water. Coffee industry is present in 80 countries and employs around 100 million people [14]. The International Coffee Organization (ICO) predicted in 2020 that coffee consumption would rise from 1.24 to 169.34 million bags in 10 years [15]. According to these statistics, a large amount of CGW will be produced, which will be released as household or industrial waste and cause environmental issues, due to their polyphenols, tannins, and caffeine contents, making them hazardous residue [16]. Coffee waste is lignocellulosic biomass, predominantly containing carbon, hydrogen, oxygen and nitrogen atoms, which form cellulose (59-63 wt%), lignin (20–26 wt%), and hemicellulose (5–10 wt%) [16]. However, because this material has already undergone a hydrothermal extraction procedure, the content of these compounds is often minimal in comparison to lignocellulosic constituents (10 wt%). Furthermore, inorganic micronutrients, such as magnesium, calcium, or salt, are commonly present in most coffee wastes, but their quantities are typically less than 5% dry weight [17].

The hygrothermal behavior of cob buildings is related to several parameters that are sometimes uncontrollable. Finding a reliable model describing the hygrothermal behavior of building is a challenging task. Indeed, their dynamics are defined by complex and non-linear processes governed by their environment. The modeling of fully coupled heat and mass transfers in building envelopes is based on several phenomenological approaches, which differ usually in the transfer potentials used. For heat transfer, in particular, the temperature is referred to a conventional transfer potential. Regarding moisture transfer, several models have been used with different mass transfer driving forces like water content [18], vapor pressure [19], vapor content [20], and relative humidity [21].

However, the main difficulty in using physical models to simulate the full hygrothermal behavior lies in the determination of the sorption curve hysteresis. Several models for hysteresis effects on moisture content have been mentioned in Hamdaoui et al. 2021 [22] to estimate the hygrothermal behavior of low-carbon buildings. The sorption hysteresis is often neglected in the standard numerical simulations at both wall and building scales. From the few models taking account of the sorption hysteresis [23], the simplified one of Mualem [24, 25] considers that no pore interactions occur and has been used in many works [26, 27].

Several numerical tools are used in the literature to take into account the hysteresis effect such as COMSOL Multiphysics, EnergyPlus and WUFI Plus. For instance Alioua et al. [21] used COMSOL Multiphysics to simulate the hygrothermal behavior of date palm concretes (DPC). They

demonstrate a better moisture transfer estimation in DPC when including hysteresis. G. Promis et al. [26] evaluated both steady and transient states, with and without moisture hysteresis effect. Hysteresis may be ignored in steady state if the relative humidity range does not surpass the capillary condensation point. However, taking into account the hysteresis increases model's complexity as well as computing cost of the simulation [28]. Furthermore, some authors show that non-hysteresis modeling can result up to 20–30% error in moisture content prediction for wood sorption behavior [29].

To achieve the optimal balance between reducing model complexity [28] and increasing accuracy, in this paper we propose a numerical analysis of the material's hygrothermal behavior using linearization of the sorption curve. In such a way, the software can improve the outputs' reliability without the need of additional equations to model the hysteresis effect. The effect of linearization of sorption curves was first validated using Alioua et al. experimental data [21]. This method is tested on a multilayer wall based on Coffee Lightening Clay (CLC) and Structural Cob (SC), for which hygroscopic, thermal, and mechanical characterization of CLC and SC are carried out at different substitution levels.

The cob materials are prepared using techniques similar to that used in traditional German and Brittany cob construction [30]. A supplementary layer is used in this construction architecture. To meet construction rules, a combination of two walling layers made of earth materials is considered. Insulation wall with a high fiber content and a load bearing layer with a greater density make up the two layers. All of the examined mechanical performances, thermal, and hydric properties of cob walls are evaluated at laboratory scale.

2 Methodology

After reviewing the relevant current literature, we divided our study into several sections, each of which being composed of multiple steps, as discussed in full in the following sections:

- Formulation and experimental characterization: Two formulations have been developed in this article: (i) Coffee Lightening Clay (CLC) and (ii) Structural Cob (SC). The hygroscopic, thermal, and mechanical characterization were carried out at different substitution levels.
- Experimental results of hygrothermal characteristics of developed materials for insulating and structural components are investigated and discussed.
- Conducting a numerical simulation campaign of the hygrothermal behavior by simplifying the modeling method and taking into account the linearized hysteresis effect: In this step, the output numerical data are vali-

Table 1 Physical properties of coffee ground wastes

	Porosity (%)	Bulk density (kg m ⁻³)	Water absorption (%)	рН
CGW	52.1	468±3	0.9	6.1 ± 0.01

Table 2 Biochemical composition of coffee ground wastes

	Weight (wt. %)
Proteins	15.3
Cellulose	26.2
Hemicellulose	23.8
Lignin	24.9
Lipids	7.7
Ashes	2.1

dated with Alioua et al. experimental data [21] at wall scale.

 Hygyrothermal performance evaluation and model testing: Once the method is validated, we test it for a doublelayer wall (CLC and SC) using WUFI Plus software.

3 Experimental setup and material elaboration

3.1 Coffee grounds waste valorization

Coffee ground wastes (CGW) are derived from mixtures of Arabica coffee species, made by Jacques Vabre (Kraft Foods Group, Paris, France). CGW were collected from our coffee bar (Caen, Normandy, France). It is important to notice that more than 2 tons of coffee grounds are generated each year in our school. As soon as collected, the raw coffee ground wastes material was dried for 24 h at 105 °C, crushed, and sieved to a particle size of 63 microns. The heating temperature of 105 °C resulted in satisfactory drying of the material. The physical properties of CGW are summarized in Table 1.

The raw coffee ground wastes were subjected to a two-step sequential acid hydrolysis to evaluate the proportions of cellulose, hemicellulose, and lignin (ash free) [31]. High-performance liquid chromatography was used to quantify the sugars in the resulting solution, which were then used to compute the cellulose (glucose), hemicellulose (arabinose, mannose, galactose, and xylose) and lignin (ash-free) contents [32]. The average values are given, and the measurement errors are estimated to less than 10%. Raw CGW (Table 2) contains mostly carbohydrates, cellulose and hemicellulose for half its weight, with lignin as the third major component. Other biochemicals are 14.2% of proteins, 9.5% of lipids and 2.1% of ash.



Inductively coupled plasma atomic emission spectrometry (ICP-AES) estimates that the most abundant elements in CGWs (Table 3) are potassium and magnesium, the former accounting for 40% of the oxide ash [33], with a total amount for these two elements of more than 60% of all CGW probed elements [32].

3.2 Natural fiber

Natural fibers were employed as reinforcement and insulators parts (Table 4). The fibers used in this study were provided by the local farmers from Laulne (Normandy). For the Structural Cob (SC), we used the wheat straws. The wheat straws fibers have a thermal conductivity between 0.035 and 0.054 W m⁻¹ K⁻¹ [5]. For the Coffee Lightening Clay (CLC) we used the reed fiber. They are readily accessible and affordable. Due to their fully biodegradable properties, as well as their weak CO₂ emissions budget compared to synthetic fibers, their commercialization could have a lower environmental impact. The usage of reed is essentially appropriate as an insulating material with a thermal conductivity close to 0.05 W m⁻¹ K⁻¹ [34].

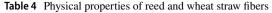
3.3 Characterization techniques

The analyses of soils composition were performed by X-ray fluorescence (XRF) technique. The Inel Equinox 3500 spectrometer was used to collect the X-ray fluorescence spectra (equipped with a Cu microfocus source, a parabolic multilayer mirror on the primary beam, and an Amptek X-123SDD Silicon Drift Detector were placed vertically 10 mm over the sample to ensure high sensitivity even with low-atomic-number elements). Data were collected with an integration time of 400 s.

X-ray powder diffraction diagram was collected using Cu K α radiation (=1.54059) selected by an incident beam Ge (111) monochromator on a D8 Advance Vario 1 Bruker instrument (2-circles diffractometer, θ –2 θ Bragg–Brentano mode). The X-ray diffraction pattern of soil is collected for

 Table 3
 Elemental composition of coffee ground wastes

Mineral	Concentration (mg/(100 g))
Potassium (K)	273±27
Magnesium (Mg)	51 ± 3
Calcium (Ca)	39 ± 3
Manganese (Mn)	1.9 ± 0.1
Copper (Cu)	1.1 ± 0.1
Sodium (Na)	1.0 ± 0.05
Iron (Fe)	0.8 ± 0.05
Zinc (Zn)	0.2 ± 0.05



	Diameter (mm)	Density (kg m ⁻³)	Initial water content (%)	Tensile strength (MPa)
Wheat straw	1–4	1408 ± 5	10.7	23.9 ± 3.5
Reed	1–4	1294 ± 5	8.5	117 ± 9

1 s each 0.01° step (16 h/scan) from 10° to 80°. The Full-Pattern Search-Match (FPSM) technique and the Crystallography Open Database [35] were used for quantification and crystalline phase identification, whereas the MAUD software [36] was used for Rietveld quantification.

Analysis of elements present in tap water was performed via The Thermo Scientific DIONEX ICS-3000 DC Ion Chromatography. The ion chromatography is composed by a dual-pump module, an eluent generator module, a chromatography detector module, and an autosampler. The device has a 1800 psi column pressure and a 1.0 mL min⁻¹ eluent flow rate. Interpolation on an appropriate calibration curve was used to identify and quantify the ionic species. All of the analyses were carried out at room temperature.

The analyses of coffee ground wastes composition were carried out using an Elan 6000 inductively coupled plasma optical emission spectrometer model Vista-Pro with axial view (Varian, Mulgrave, Australia). The emission intensities for the most sensitive lines were measured without spectral interference.

3.4 Structural earth

The structural earth used in this study contains mainly silicon, aluminum, iron, and sodium for the major cations (Table 5) XRD analysis is very important to characterize the

Table 5 Chemical composition of structural soil obtained by EDX measures

Element	Wt.%
Silicon dioxide (SiO ₂)	65.89
Aluminum oxide (Al ₂ O ₃)	14.23
Ferric oxide (Fe ₂ O ₃)	6.65
Magnesium oxide (MgO)	4.08
Potassium oxide (K ₂ O)	2.17
Titanium dioxide (TiO ₂)	2.08
Calcium oxide (CaO)	1.27
Sodium oxide (Na ₂ O)	1.11
Manganese oxide (MnO)	0.16
Phosphorus Pentoxide (P ₂ O ₅)	0.14
Sulfur trioxide (SO ₃)	< 0.1
Loss on ignition	2.26



mineralogical composition of soils. For instance, Si atoms can be found in quartz or clays, two phases with quite distinct properties when used in Cob. The online Full-Profile Search-Match fitting process (FPSM, http://nanoair.dii.unitn. it:8080/sfpm/) was used to do a preliminary quick phase analysis. The FPSM tests all probable crystal structures from the COD Database (limited to the XRF-detected elements) using a Rietveld fitting process, resulting in an ordered list of candidates for further quantification. The soil's XRD pattern is then Rietveld-fitted, with the preceding phase identification taken into account. The general R-factors indicate the overall goodness of fit between the model and experimental data are: Rwp = 5.3% and Rb = 3.9%, giving goodness of fit of 1.8. The microstrain values are also fitted during this step and remain low for all the phases.

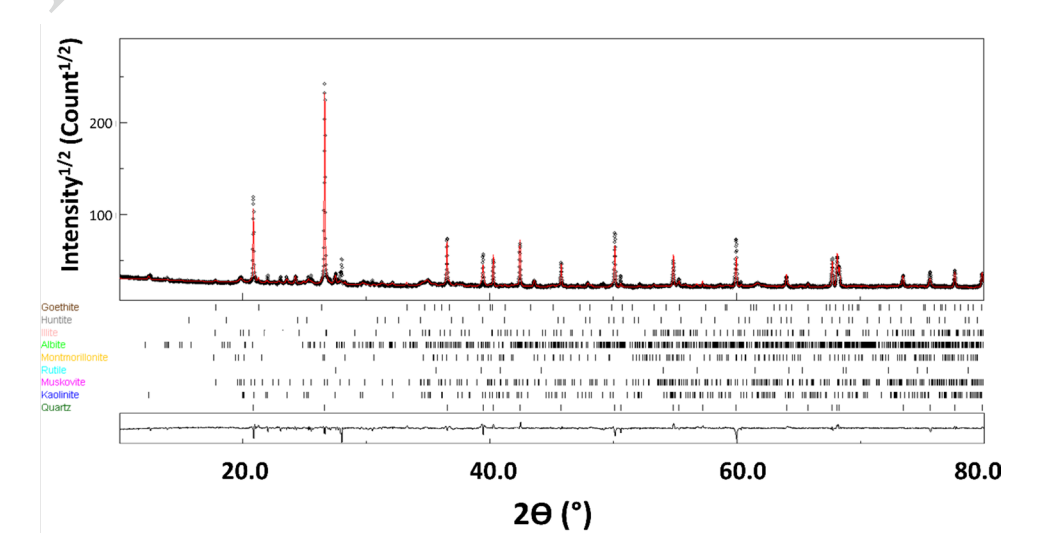
According to the quantitative phase analysis using Rietveld refinement, the XRD diagram is indexed by the following major phases: quartz (66.7%), muscovite (26.2%), montmorillonite (6.9%) and albite (4.2%), with minor occurrences of Kaolinite, goethite, rutile, illite, and huntite (Fig. 1, Table 6).

Quartz usually forms under rocks ignition. Quartz is composed of silica tetrahedra, with all oxygen atoms bonding to all silicium atoms covalently [37]. This results in a tremendously strong crystal with no weak planes [37]. Muscovite (also known as common white mica) is a hydrated aluminum–potassium phyllosilicate mineral. It possesses a nearly complete basal cleavage, resulting in incredibly thin laminae (sheets) that are frequently quite elastic. [5]. Montmorillonite is an aluminum silicate mineral with hydrated magnesium. Montmorillonite, often known as TOT (Tetrahedron/Octahedron/Tetrahedron), is a 2/1 type clay. Each montmorillonite sheet consists of three layers: an octahedral layer of Al(OH-)₅O and two tetrahedral layers of SiO₄ [5]. The ability of montmorillonites to swell when water fills the area between the layers is one of its most remarkable

properties. Montmorillonite dispersed in water produces a stable colloidal suspension relatively quickly. On the other hand, this ability to swell and shrink (collapse of the clay layers during desiccation) causes substantial geotechnical issues, generating sometimes significant displacements at foundations due to fluctuations in sub-soil humidity. Albite is a feldspar mineral (silicate group, tectosilicate subgroup) with the formula NaAlSi₃O₈ and can contain traces of calcium, potassium, and magnesium [5]. Goethite is an iron (III) oxyhydroxide mineral, specifically the α polymorph of the FeO(OH) compound [5]. Goethite forms through weathering of other iron-rich minerals. Kaolinite is a mineral composed of hydrated aluminum silicate and belongs to the phyllosilicates subgroup (Kaolinite-serpentine group) [5]. Rutile is an oxide mineral, the most abundant natural form of TiO₂. Rutile is a frequent accessory mineral in metamorphic and igneous rocks with high temperatures and pressures [38]. Illite refers to a category of clay minerals that do not swell. Illite species are made up of three layers of phyllosilicates, with one layer of aluminum (Al) sandwiched between two layers of silicate (SiO₄). Bisiallitization, a reaction that occurs when water is attacked under particular temperature and pressure circumstances, produces micas (muscovite, biotite) and other silicates (feldspar, feldspathoids, orthosis, and others) [5]. Huntite is a carbonate mineral formed at low temperature. Huntite is a surface weathering product of magnesium-rich rocks such as serpentinites, or magnesite [39].

Some clays have the potential to expand the interfoliar gaps between their leaves. The insertion of hydrated cations (Na, Ca, etc.) gives rise to this feature, which allows charge compensations between layers [40]. If the clay charge is too high (e.g., micas or muscovite in our sample: total clay charge of -1 fully counterbalanced by the dehydrated cations (K⁺)), the phenomena disappears (e.g., pyrophyllite, talc: total clay charge of 0, no interfoliar cation). The

Fig. 1 XRD pattern of structural soil. Observed (black dots) and computed (red line) patterns are represented, together with the difference curve ($I_{\rm obs}-I_{\rm calc}$)



Springer

Table 6 Refined values of lattice parameters, unit cell volume, average isotropic crystallite sizes < D> and microstrains < ϵ^2 > $^{1/2}$

Phases	COD reference	V (%)	Lattice type + Space group	Lattice parameters (Å)	$\langle D \rangle$ (nm)	$\langle \epsilon^2 \rangle^{1/2}$
Quartz	1,526,860	54.8 (5)	Trigonal	a=4,914 (2)	492 (10)	5. 10 ⁻⁴
${ m SiO_2}$			P3 ₂ 21	c = 5,405 (2)		
Muscovite	1,100,011	26.2 (5)	Monoclinic	a = 5,194(1)	35 (5)	6. 10^{-3}
$KAl_2(AlSi_3O_{10})(F,OH)_2$			C2/c:b1	b = 9,005(2)		
				c = 19,995(1)		
				$\beta = 95.782(1)$		
Montmorillonite	1,100,106	6.9 (2)	Monoclinic	a = 5,386 (2)	111 (6)	6. 10 ⁻⁴
$(Na,Ca)_{0.3}(Al,Mg)_2Si_4O_{10}(OH)_2$			C2/c:b1	b = 9,039(2)		
				c = 10,196(2)		
				$\beta = 100.457 (2)$		
Albite	1,556,999	4.2 (2)	Triclinic	a = 8,166(1)	43 (5)	6. 10^{-3}
NaAlSiO ₃			P1	b = 12,845 (1)		
				c = 7,188(1)		
				$\alpha = 94.240(1)$		
				$\beta = 116.590 (1)$		
				$\gamma = 87.715$		
Kaolinite	1,011,045	2.1 (3)	Monoclinic	a = 5,185(1)	78 (5)	6. 10 ⁻⁴
$Al_2Si_2O_5(OH)_4$			Cc:b1	b = 8,885 (1)		
				c = 14,526 (1)		
				$\beta = 100.662 (1)$		
Goethite	2,211,652	2.0(3)	Orthorhombic	a = 4,579(1)	21 (1)	6. 10 ⁻⁴
α-FeO(OH)			Pbnm: cab	b = 9,945(1)		
				c = 2,998 (1)		
Rutile	1,532,819	1.6 (3)	Tetragonal	a = 4.582(1)	92 (5)	8. 10 ⁻⁴
TiO_2			P42/mnm	c = 3.014(2)		
Illite	2,300,190	1.1 (2)	Monoclinic	a = 5,197(1)	100 (5)	6. 10 ⁻⁴
${\rm (K,H_{3}O)(Al,Mg,Fe)_{2}(Si,Al)_{4}O_{10}[(O}$			C2/m:b1	b = 8,961 (1)		
$H)_2,(H_2O)]$				c = 10,159(1)		
				$\beta = 100.970 (1)$		
Huntite	1,000,046	1.1(2)	Trigonal	a = 9,502(2)	123 (5)	8. 10 ⁻⁴
$Mg_3Ca(CO_3)_4$			R32:H	c = 7,821(2)		

One standard deviation is indicated in parenthesis on the last digit

subclass of smectites is among the expandable species, with a charge ranging from 0.3 to 0.8. The water inserted via the hydrated cations is what permits the crystalline structure to enlarge [40]. Due to excessive humidity, the swelling becomes even more critical. With a rate of 6.9%, montmorillonite is the only expandable species found in our soil. The shrinkage properties of our soil will be influenced by the presence of muscovite, albite, kaolinite and illite. Because of their small interfoliar space, these crystals have few water molecules between their layers [40]. As a result, when submerged in water, they have little intercrystalline swelling [46] and these four phases shrink far less while drying than smectite clays like montmorillonite [38]. The major minerals in both sandy and silty soils are primary minerals, which means they are remnants of the minerals in the original

parent material. The quartz is the first weather-resistant mineral formed. Mica, feldspars, iron oxy-hydroxides, and limonite are other minerals that are commonly found, though in smaller concentrations [41].

In conclusion, the structural soil used for structural cob is typical of silty soil. Indeed, it is constituted of non-altered minerals: grains of quartz and silicates (micas, feldspars, smectites and serpentines).

3.5 Lightened earth

The lightened earth is composed of kaolinite and illite with trace of chlorite. When combined with water, kaolinite gives the clay its moldability [42]. Table 7 shows the chemical



Journal : Large 43452	Article No : 579	Pages : 26	MS Code : 579	Dispatch : 24-12-2022	
-----------------------	------------------	------------	---------------	-----------------------	--

Table 7 Chemical composition and mechanical properties of lightened earth

Element	Wt.%
Silicon dioxide (SiO ₂)	59.73
Aluminum oxide (Al ₂ O ₃)	20.25
Ferric oxide (Fe ₂ O ₃)	6.09
Calcium oxide (CaO)	5.33
Magnesium oxide (MgO)	3.16
Sodium oxide (Na ₂ O)	0.1
Potassium oxide (K ₂ O)	2.05
Sulfur trioxide (SO ₃)	< 0.1
Phosphorus Pentoxide (P ₂ O ₅)	< 0.1
Cl ⁻	0.18
Loss on ignition	3.10
Physical properties	
Plasticity limit (%)	42.5
Plasticity index (%)	15.3
Absolute density (g.cm ⁻³)	2.73

composition and mechanical characteristics of the used lightened earth.

3.6 Soils preparation

To eliminate the absorbed water, the soils were dried in hot air oven at 105 °C for 24 h before being milled to a fine powder (<63 µm). Previous research indicates that the earth has a greater particle size distribution. When producing the earth for the preparation of mixture, lightened and structural earth particles with diameters less than 2 mm must account for around 98 percent of total particles. Coffee lightening clay (CLC) and Structural Cob (SC) are bio-based composites composed of common natural materials. The insulating component is formed of cob, sand, fiber, and CGW, while the structural part is made of Clay, sand, fiber, and CGW. Local tap water with a pH of 7.68 (Table 8) was used to mix SC with coffee ground wastes (Table 9).

The soil-fiber-CGW mixtures with the optimum thermal characteristics were chosen for this investigation. As a result, a blend of 20% coffee ground wastes for CLC and 0% for SC was chosen (Table 9). Indeed, the addition of CGW in the SC material shows a very low compressive strength compared to the standard Cob. This effect is due to the nature of soil used which is silty soil with very low amount of calcium.

No fracture was observed in our specimens, and after 28 days, their shrinkage was less than 1%. Since the thermal conductivity of the 20 wt% sample was the lowest $(0.14 \text{ W m}^{-1} \text{ K}^{-1})$, we then decided to select this latter for the following investigation.

Table 8 Chemical composition of tap water and seawater used in concrete mixtures

Concentra- tion in mg/l
88.7
38.4
42.9
52.0
9.1
2.6
0.3
0.2
< 0.1
< 0.1
< 0.1
8.4
5.2

3.7 Material properties measurement

The mathematical models employed in this study require as input a collection of material attributes such as sorption isotherms, vapor resistance factors, thermal conductivity, heat capacity, and so on, to undertake numerical research on the hygrothermal behavior of CLC/SC multilayered wall. As a result, these parameters were determined experimentally in accordance with international standards, as detailed in the following subsections.

Water vapor permeability, porosity, and vapor resistance factor

Water vapor permeability describes a hygroscopic wall's capacity to enable vapor transport under relative humidity variations. Many experiments were performed to estimate vapor resistance factors: dry cups (NF EN ISO 12572) [43] corresponding to relative humidity ranges of 0%–50%. The basic idea behind this test is to induce relative humidity gradients between the two sides of a sample that is sealed laterally, and then monitor the daily mass fluctuation until it becomes constant. The porosity was calculated using the NF ISO 5017 standard [44].

The specimen's mass change is monitored until it reaches constant mass. The following formulae were used to compute the water vapor permeability and resistance factor of hygroscopic low-carbon material:

Water vapor flow rate $G = \frac{m_2 - m_1}{t_2 - t_1}$ (kg s⁻¹), where m is the specimen's weight at time t.

Table 9 Mixture proportion of the developed structural and insulating wall parts made of coffee ground wastes

	Coffee lightened clay (CLC)				
	0%	5%	10%	15%	20%
Lightened clay	1	0.95	0.9	0.85	0.8
Coffee grinds	0	0.05	0.1	0.15	0.2
Reed	0.25	0.25	0.25	0.25	0.25
	Structural Cob	(SC)			
	0%				
Structural cob	0.67				
Coffee grinds	0				
Sand	0.33				
Straw	0.02				

Water vapor permeance $w = \frac{G}{A \Delta P_v} (\text{kg m}^{-2} \text{ s}^{-1} \text{ Pa}^{-1}), \text{ where}$ 451

- ΔP_y is the water vapor pressure difference across specimen, 452
- A is the area of specimen. 453

458

459

460

461

462

464

465

466

467

468

469

470

471

472

473

474

475

476

478

479

- 454
- Water vapor resistance $z = \frac{1}{w} (\text{m}^2 \text{ s Pa kg}^{-1})$. Water vapor permeability $\delta = w d (\text{kg m}^{-1} \text{ s}^{-1} \text{ Pa}^{-1})$, where 455
- d is the mean thickness of specimen. 456
- Water vapor resistance factor $\mu = \frac{\delta_{air}}{s}$. 457

Thermal conductivity, heat capacity, and dry density

Thermal conductivity changes with coffee ground wastes fraction (CGW) and temperature (T) for the insulating part. The following equation was used to simulate thermal conductivity as a function of (CGW) and (T) in this work:

$$\lambda = [0.1511 (CGW)^{-0.016} + 1.9 \cdot 10^{-3} (CGW)^{0.984} - 1.2 \cdot 10^{-4} (CGW)^{1.984}] \left(\frac{T}{T_{ref}}\right)^{0.068},$$
(1)

Where T_{ref} is equal to 10 °C and T in the mean ambient temperature in °C and CGW is the fraction of coffee ground wastes (between 0 and 1).

This equation can ease straight determination of the thermal conductivity of the insulating part as a function of temperature and CGW content, either for an experimental inquiry or for numerical calculations of energy performance.

The ability of a cob wall to store thermal energy is measured by its specific heat capacity (Cp) at constant pressure. Cp measurements were done using the Differential Scanning Calorimetry method (DSC, NETZSCH STA 449 F3), which follows the ISO 11357–4 standard [45]. Data have been collected from – 20 °C to 30 °C, with a heating rate of 1 °C min⁻¹.

The BET technique was used to calculate the specific surface area of the cob specimens, and a helium pycnometer

was used to determine the absolute density of all raw materials (Accupyc II 1340).

481

482

483

484

485

486

487

488

489

490

491

492

493

494

495

496

497

498

499

500

501

502

503

504

505

506

507

Sorption isotherm curve

Due to the obvious great porosity of vegetal fibers, the sorption isotherm of bio-based materials is an extremely essential property. This particular curve illustrates the evolution of water content in the whole material as a function of relative humidity change and at a certain temperature of the specimen based on the norm NF EN ISO 12571 [46]

4 Results and discussion

4.1 Mechanical and hygrothermal properties

To assess the hygrothermal efficiency of our constructed earth walls, we reviewed and compared our data to experimental data obtained for various earth fiber materials such as lightened earth and clay of varying densities. The next subsections provide the determined thermal conductivities, densities, specific heat capacities, and isothermal sorption curves. Despite the fact that all of the findings are from the same material, the hygroscopic values for the insulating parts vary greatly compared to the structural part.

4.1.1 Hygrothermal properties of the structural part (structural cob. SC)

Table 10 summarizes all the hygrothermal properties of the SC materials necessary either to experimentally investigate their behavior or when launching numerical simulations.

The moisture sorption curve for the used SC material exhibits a type II-isotherm behavior [47] with a sigmoidal shape (Fig. 2). Such a behavior is obviously linked to the



Journal : Large 43452 Article No : 579 Pages : 26 MS Code : 579 Dispatch : 24-12-202:	Journal : Large 43452	Article No: 579	Pages : 26	MS Code : 579	Dispatch : 24-12-2022
---	-----------------------	-----------------	------------	---------------	-----------------------

porous nature of this material and similar to earth-fiber-containing cobs.

SC material shows a moisture content nearly two-third that of CLC (Fig. 4), thanks to a lower porosity in the latter, and as expected for an insulating component compared to a structural part.

4.1.2 Hygrothermal properties of the insulating part (coffee lightened clay—CLC)

The thermal conductivity of the clay specimens without CGW addition ranges between 0.169 and 0.188 W m $^{-1}$ K $^{-1}$ for temperatures from 10 °C to 40 °C (Fig. 3a). Upon 10% CGW addition, such values decrease from 0.169 W m $^{-1}$ K $^{-1}$ to 0.156 W m $^{-1}$ K $^{-1}$ in the same temperature range.

These results show that incorporating CGW into the earth matrix reduces the thermal conductivity of the CLC. The most effectively tested CGW content for enhancing the material's thermal insulation appears to be the maximum tested addition of 20%. Compared to ordinary cob, the addition of 20% CGW reduced thermal conductivity by 24.2% at 10 °C and 24.5% at 40 °C CLC exhibited apparent porosity values that varied from 46 to 63% (Fig. 3b), with a simultaneous bulk density decrease of the material by about 26% (Fig. 3c). The decrease in density of CLC is obviously due to the added amount of coffee waste, since the density of CGW is much lower than that of cob, resulting in a valuable weight decrease at the construction stage. The addition of CGW to cob results in an enhanced porosity helping the reduction of thermal conductivity of the specimens. Pores are filled by air in our case, with a much lower thermal conductivity than the solid materials of concerns, reducing the conductivity of the samples.

At 10 °C, the thermal conductivity values decreased by up to 24.2%, indicating a greater potential for energy savings in residential applications. The thermal conductivities of the samples are obviously connected to their densities and porosities, as we observed, and further integration of CGW in the CLC could be studied to better investigate this effect.

According to the NF ISO 5017 standard [44], porosity is evaluated by quantifying the weight of a dry test piece, its apparent mass when submerged in a solution with which it has been soaked under vacuum conditions, and its mass in air while still saturated with the liquid. We notice a porosity

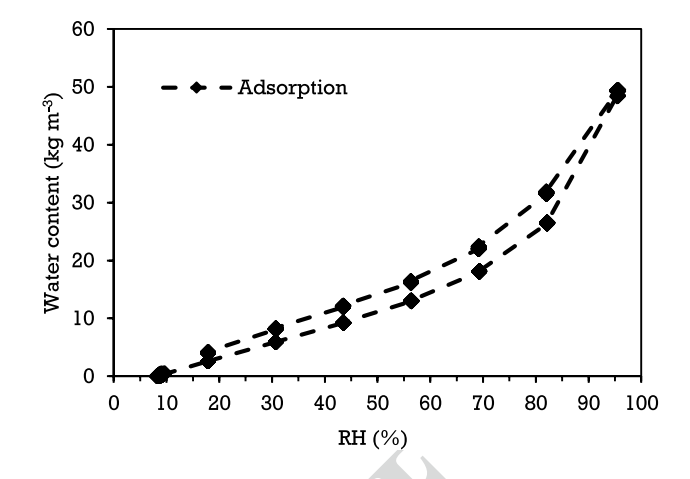


Fig. 2 Sorption curve of Structural Cob (SC with 0% of coffee ground wastes)

increase from 0.45 without CGW in the CLC wall to about 0.63 (Fig. 3b) for 20% of CGW in the formulation design (Table 9), representing an increase of 40%.

The specific heat capacity (Fig. 3d) also increases with the amount of CGW, reaching around 1075 J kg⁻¹ K⁻¹ for 20% in CLC, an exceptionally large value compared to the earth–fiber combination. Materials with larger specific heat capacities are typically required to enhance construction's insulation applications. As far as Cp values are concerned, our measurements show that soil–fiber–coffee mixtures perform better than typical cobs with simple soil–fiber combinations.

The moisture sorption curves for all CLC specimens are very similar (Fig. 4) and exhibit type II-isotherm behavior [47] as usual for characteristics of porous materials, and as observed in ordinary cobs. The water content decreases slightly upon addition of CGW in the specimens. This can be explained by a variety of causes, including the porosity of the sample, which can significantly affect the interaction patterns of water molecules inside the micropores. Understanding properly the adsorption/desorption behavior can lead to an accurate hypothesis when we need to derive the diffusion of water inside porous media based on a different approach such as Knüdsen model. It is recommended to always rely on the experimental investigation of these

Table 10 Hygrothermal properties of Structural Cob (SC 0%)

Property	Value	Property	Value
Dry density ρ (kg m ⁻³)	1384	Dry specific heat <i>Cp</i> (J kg ⁻¹ K ⁻¹)	865.2
Dry thermal conductivity λ (W m ⁻¹ K ⁻¹)	0.33 at 10 °C	Porosity	0.34
Vapor resistance factor (dry cup) μ [-]	8.385	Water vapor permeance $w \text{ (kg m}^{-2} \text{ s}^{-1} \text{ Pa}^{-1})$	3.518 10 ⁻¹⁰



Journal: Large 43452 Article No: 579 Pages: 26 MS Code: 579 Dispatch: 2	Dispatch : 24-12-2022
---	-----------------------

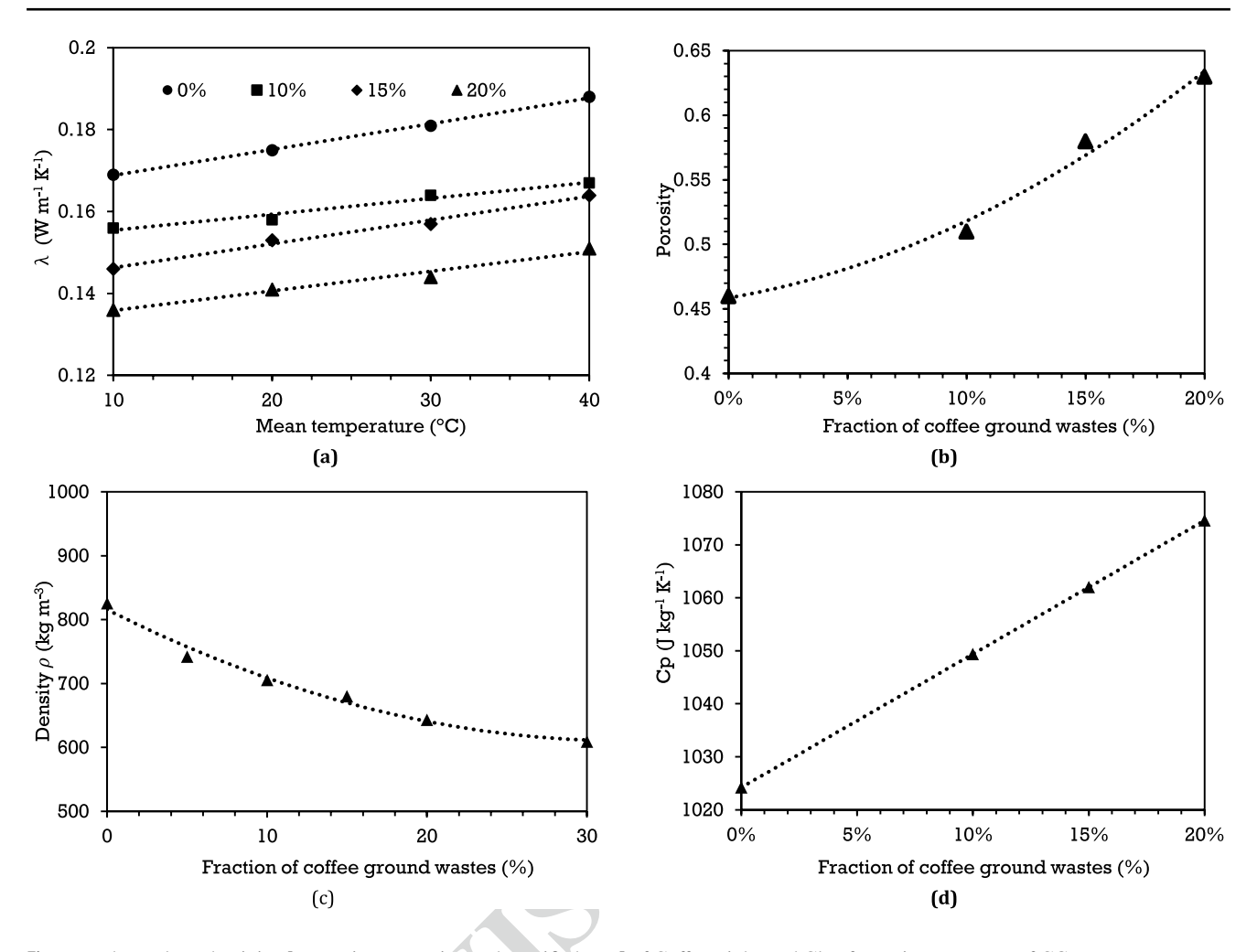


Fig. 3 a Thermal conductivity, b Porosity, c Density, and specific heat d of Coffee Lightened Clay for various amounts of CGW

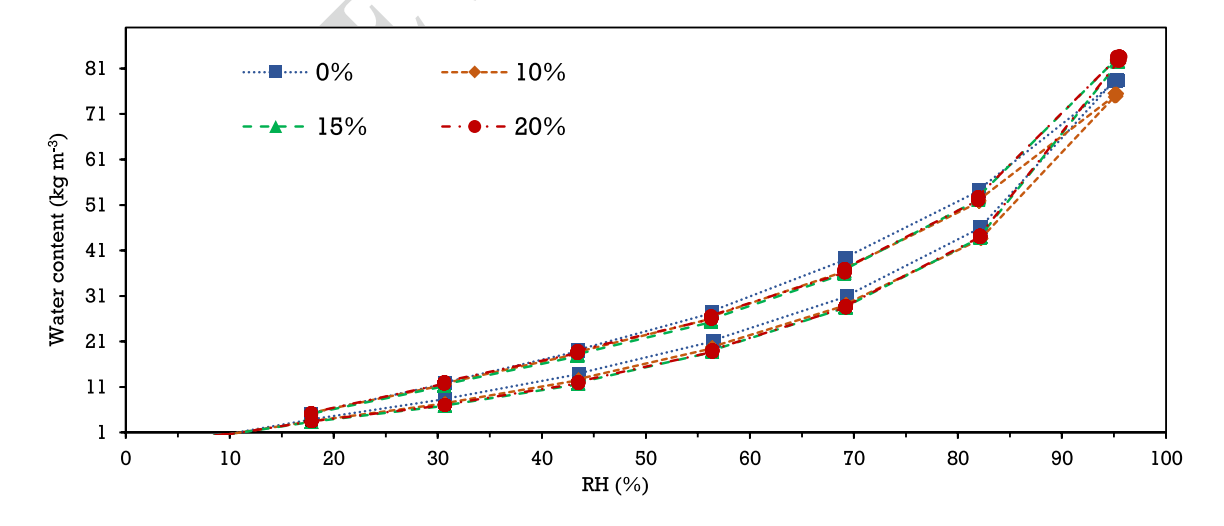


Fig. 4 Moisture sorption isotherm curve of Coffee Lightened Clay for different portions

parameters because the phenomenon behind it is a rather complicated to understand completely.

CLC and SC like other bio-based construction materials are very hygroscopic and absorb far more water than



576

Journal : Large 43452	Article No: 579	Pages : 26	MS Code : 579	Dispatch : 24-12-2022

traditional construction materials. CLC has low density and large porosity, resulting in good hygric characteristics and insulating capacity. The increase in coffee waste fraction leads to a decrease in water vapor resistance factor, from 6.1 to 5.5 (Fig. 5).

The capacity of bio-composites to transmit water vapor under varied relative humidity situations is determined by their water vapor permeability. The water vapor permeability tests were carried out in accordance with NF EN ISO 12571 [46]. The samples were sealed with molten wax and aluminum sheets on both sides, then the difference in relative humidity between their inner and outer surfaces recorded.

The water permeability (δ) of CLC samples increases progressively and linearly with the amount of incorporated coffee grounds (Fig. 6), from typically 2.97 10^{-11} kg m⁻¹ s⁻¹ Pa⁻¹ to 3.27 10^{-11} kg m⁻¹ s⁻¹ Pa⁻¹ for 0% and 20% CGW, respectively.

4.1.3 Material compression strength

All the dry components were mixed up to homogeneity before water was progressively added while continuously mixing until a homogenous fresh composite mix was obtained. The mix was then progressively formed layer by layer in either cylindrical or parallelepiped molds (see Fig. 7), with care taken to avoid the formation of cavitation or unfilled gaps in the encased shell. The constructed blocks were removed from the molds one day later. Drying in the laboratory was operated for one month at conditions of 50% RH and 20 °C. Temperature and relative humidity were recorded on a regular basis during the drying step to ensure they remained stable.

Apart from the absence of adhesion between the mixture's ingredients, no particle breakage was seen in the compression tests performed on the cylinders. Consequently, the

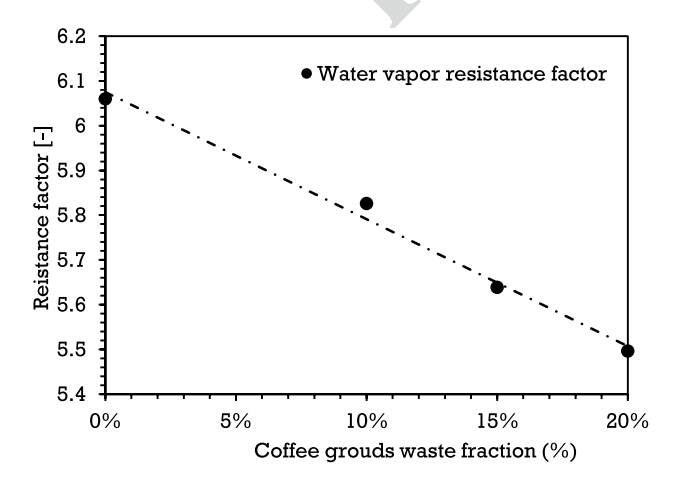


Fig. 5 Water vapor resistance factor of CLC samples upon CGW additions

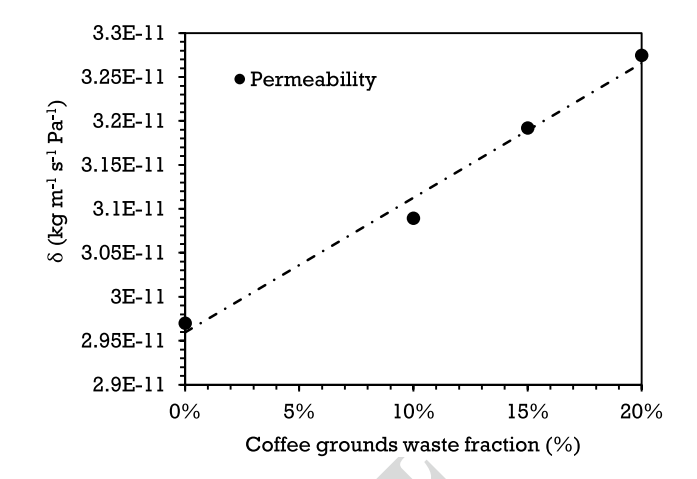


Fig. 6 Permeability of CLC samples upon CGW additions

compressive, apart from the absence of adhesion between the mixture's ingredients, no particle retraction was seen in the compression tests performed on the cylinders. Consequently, the compressive strength of these developed materials cannot reach the maximum recorded stress. A previous study revealed the maximum compressive strength for a percentage of longitudinal deformation ranging from 1.5 to 7.5%. Cob (Fig. 8b) exhibits a maximum compression stress of 1.2 MPa from 2 to 4% of deformation. As expected, the insulating but not structural cob composite reaches such deformation levels for 5-10 times less stresses. However, incorporation of up to 15% of CGW significantly increases the compression strength (Fig. 8a), while the CLC sees its thermal conductivity decreasing (Fig. 3a)). The CGW incorporation then favors simultaneously mechanical and insulating properties.

The compression tests were carried out using a Schenck 4-column press, equipped with a hydraulic cylinder and able to perform traction, compression, shear, and flexion tests with force values up to 3000 kN. It is mostly used for mechanical testing of construction materials applied on 11 diameter × 22 heights cm cylindrical samples. The test setup was based on a displacement speed of 0.05 kN/s and a maximum displacement height of 10 cm.

The mixes of CLC with 15% CGW also show the largest strength after larger deformations, up to 5%, compared to other specimens (Fig. 8a). This behavior is due to the better adhesion between the ground, fibers, and lignin present in CGW, which stops fracture propagations. Lightened earth is known to undergo differential settlements and low shear strength and must be consolidated in order to enhance its mechanical properties. Finally, the stabilizing effect of CGW in this study could be attributed to lignin, this latter being the only component of the coffee biomass that includes no carbohydrates and is responsible for its rigid structure [48].



Fig. 7 Coffee lightened clay (red) and Structural cob (brown) samples used for mechanical (Ø11 cm×22 cm) and thermal (30×30×4 cm) tests

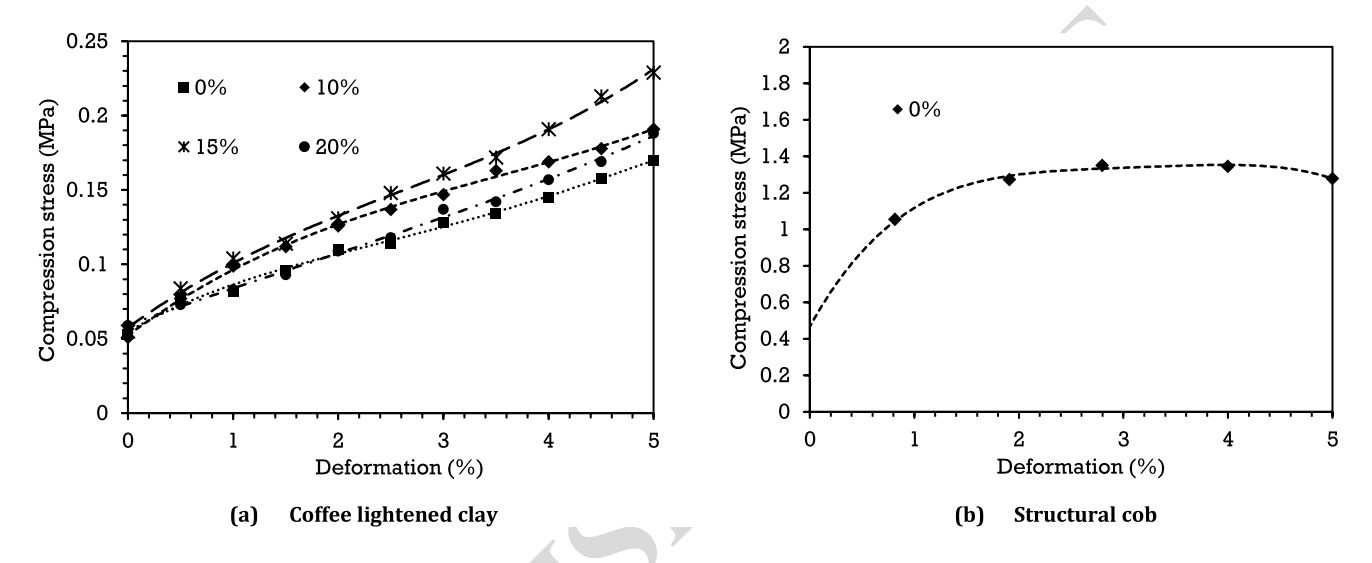


Fig. 8 CLC (a) and SC (b) compression strength tests as a function of deformation

The amount of lignin in the CGW is around 24.9% of the dry weight of the biomass (Table 2). Due to its ability to absorb and hold a high quantity of water inside its structure, lignin is regarded a non-carbohydrate-based polymer that is a particularly important hydrophilic substance. Hydrolytic depolymerization of lignin results in lower molecular weight molecules with lower alkyl-aryl ether and larger phenolic OH contents [49]. The mass change for CLC 20% and the CLC 0% specimens are roughly 82 kg m⁻³ and 78 kg m⁻³, respectively, at 95% RH, which is of special relevance (Fig. 4). The adsorption curve value at 95% RH for SC specimen is close to 50 kg m⁻³ which is almost equal to 60% of the CLC material total adsorption capacity at the same relative humidity (Fig. 2).

Our results are in agreement with Sena da Fonseca et al. (2014) [50] who investigated the use of CGWs in clays for the production of ceramic bricks. For the ceramic samples, clay pastes containing 5, 10, 15, and 20% CGWs were examined. It was found that adding CGW to the mix increased perceived porosity and water absorption. The thermal conductivity of the samples was also reduced with incorporation

of CGWs. The addition of 20% CGW, for example, lowered thermal conductivity by 70%. The replacement of clay by CGW to produce clay bricks was also studied by Eliche-Quesada et al. (2011) [51]. The use of CGW up to 2% resulted in open cell porosity in the bricks, which reduced thermal insulating. However, the use of CGWs at higher concentrations (3–5%) resulted in lower density and higher porosity (closed-cell porosity), which provided higher insulating capacity and appropriate mechanical resistance. The addition of CGW produces a decrease in density, increasing the open porosity of the clay but normally leads to a decrease in the compressive strength of the samples as the amount increases compared to the pristine specimen. However, according to our results, the addition of CGW up to 15% leads to an increase in compressive strength. Biopolymers, such as lignin, have been known as soil conditioners and stabilizers, which can improve the mechanical strength and water stability of soil aggregates [10]. By introducing the polymer at strategic locations into pores of a specific size range, their effectiveness can be greatly increased [10]. The larger the molecule, the more effective it is at stabilizing 669

670

671

672

673

674

675

676

677

678

679

680

681

682

683

684

685

686

687

688

689

 $\underline{\underline{\mathscr{D}}}$ Springer

648

649

650

651

652

653

654

655

656

657

658

659

660

661

662

663

664

665

666

667

668

soil aggregates, as one might expect. For these reasons, we believe that lignin penetrates into the pores as they expand with the addition of CGW in our CLC specimens, resulting in an enhancement of compression strength.

4.2 Numerical simulation of hygrothermal behavior

4.2.1 Geometry, boundary conditions, and mesh generating

The hygrothermal behavior simulations are operated in a 2D geometry (Fig. 9), on which boundary conditions on a precise enough mesh are described. Any CAD (Computer-Aided Design) software, used for the pre-processing procedure, must have the adaptable numeric format in order to produce the appropriate geometry and boundary conditions and to perfectly match with the energy simulation software needs.

The geometric data generated in "Native CAD" format must be changed to a format compatible with the WUFI Plus application, such as WPS. All pre-processors of building energy simulation software can read CAD data in different formats. The program must list the format as one of the eligible formats.

The boundary conditions of any fundamental issue are used to establish the upper and lower bounds of the field variables. These are the operational conditions that regulate the characteristics of these parameters. A decent set of boundary conditions is just as important as a great test setup. Subjectively, a boundary condition indicates that "it is known what happens" on a specific frontier as shown in Figs. 9 and 11 in terms of temperature and relative humidity variations at the defined outside surface boundary condition.

We used two different climatic condition profiles to validate our model (Fig. 10, taken from [21]), imposing time fluctuations in temperature and relative humidity to the external surfaces of the walls, with applied periodicities of 95 h and 500 h, respectively. The inside surfaces were exposed to constant ambient conditions (T = 23 °C and RH = 50%).

At the boundary, we are restricted by the experimental setup's constraints, ensuring that the theoretical condition is compatible with the actual simulations' arrangement.

In this work we consider the case of heat and mass convection transfers at boundaries, neglecting radiative exchanges and rain loads on the inner and outer walls. The Neumann boundary conditions are written as follows.

Inside surface:

$$-\lambda \left. \frac{\partial T}{\partial x} \right|_{out} = h_{c,out} \left(T_{air,out} - T_{surface,out} \right) \tag{2}$$

$$-\delta_{p} \frac{\partial P}{\partial x} \bigg|_{out} = \beta_{v,out} \left(P_{vap,air,out} - P_{vap,surface,out} \right) \tag{3}$$

Outside surface:

$$-\lambda \frac{\partial T}{\partial x}\Big|_{in} = h_{c,in} \left(T_{air,in} - T_{surface,in} \right) \tag{4}$$

$$-\delta_{p} \frac{\partial P}{\partial x} \bigg|_{in} = \beta_{v,in} \left(P_{vap,air,in} - P_{vap,surface,in} \right) \tag{5}$$

 δ_p is the water vapor permeability of the porous material, h_c is the convective transfer coefficient. The water vapor convection coefficient β_v is defined automatically by the WUFI software based on the wall quality and rugosity.

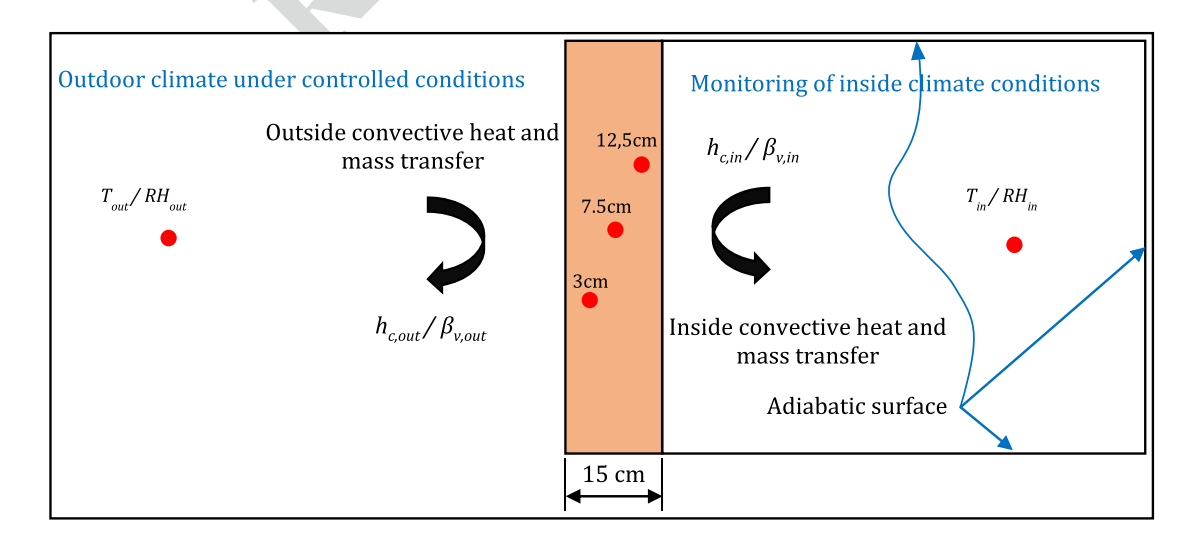


Fig. 9 Scheme of geometry and boundary conditions for numerical simulation



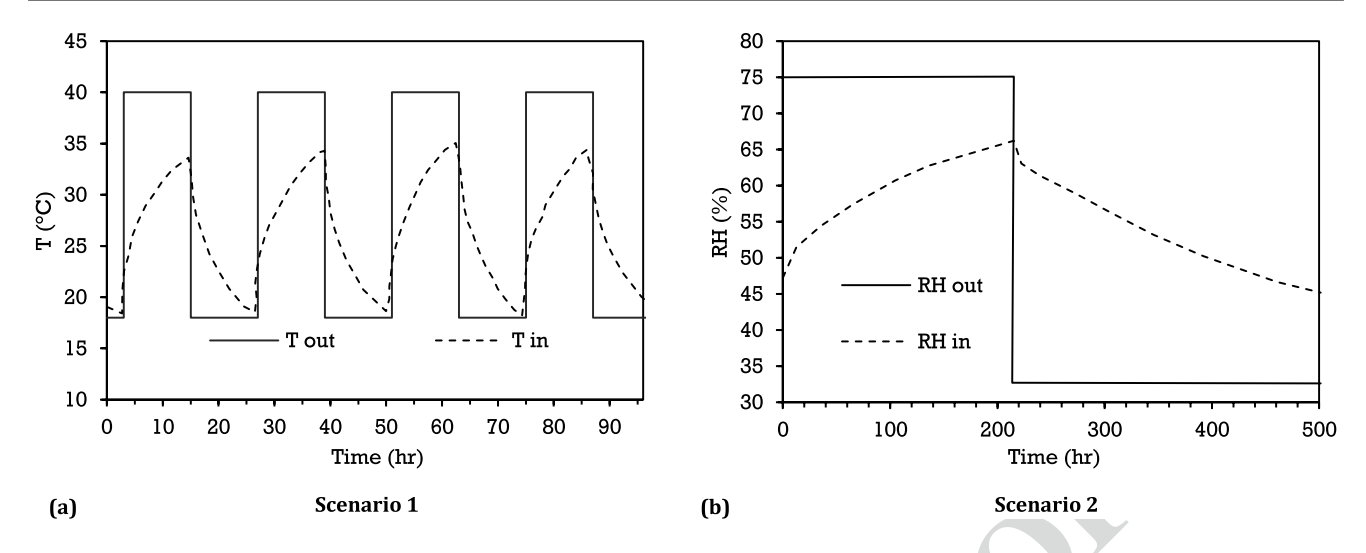


Fig. 10 Outdoor and indoor climatic boundary conditions for the isothermal (RH=50%) and isohydric (T=23 °C) scenario, Alioua et al. [21] (Refitted from original)

Outside wall Inside Wall

Fig. 11 1D wall meshing along the X axis

The starting state of the system is at initial equilibrium with 23 °C and 50% RH. External conditions are then applied in accordance to the T and RH scenario, while the inside variables are released. Before commencing any simulation, the system is always reconditioned to its initial boundary conditions (23 °C and 50% for T&RH).

We used a 1D meshing for the simulation of temperature and humidity gradients inside the hygroscopic wall (Fig. 11). The mesh step is not constant to represent this gradient with the same level of accuracy near the boundaries and farer from them. Small cells or elements are automatically created by the software to fill the volume to simulate the coupled heat and moisture transfer (Fig. 11). They form a mesh, with each cell representing a separate region that represents the temperature and humidity locally. Creating a high-quality mesh is critical for obtaining accurate solutions and ensuring numerical stability. In the case of auto-generating, software engineers guarantee that a good mesh number is generated so that the solution's stability and convergence can be efficiently attained.

4.2.2 Mathematical modeling and sorption linearization due to hysteresis effect

Künzel model

In our case study, the modeling approach simulates the hygrothermal behavior of hygroscopic building envelopes based on the Künzel model. These latter attempts to use the terms of relative humidity Φ and temperature T gradients as the primary driving forces to describe the coupled heat and moisture transfers in building components [52]. The used mass transport and heat transfer model equations are written as:

$$\frac{dw}{d\phi}\frac{\partial\phi}{\partial t} = \frac{\partial}{\partial x} \left(D_{\phi} \frac{\partial\phi}{\partial x} + \delta_{p} \frac{\partial}{\partial x} (\phi \, p_{sat}) \right) \tag{6}$$

where $(dw/d\Phi)$ is the moisture storage capacity of the porous material which can be determined from the moisture sorption curve of the considered material, D_{Φ} is the liquid

 $\underline{\underline{\mathscr{D}}}$ Springer

diffusion coefficient, δ_p is the water vapor permeability of the porous material, Φ is the relative humidity and p_{sat} is the water vapor saturation pressure.

$$\frac{dH}{dT}\frac{\partial T}{\partial t} = \frac{\partial}{\partial x}\left(\lambda_T \frac{\partial T}{\partial x}\right) + h_v \frac{\partial}{\partial x}\left(\delta_p \frac{\partial}{\partial x}(\phi \, p_{sat})\right) \tag{7}$$

where (dH/dT) is the heat storage capacity of the porous material, λ_T is the thermal conductivity and h_v is the evaporation enthalpy of water.

Hysteresis effect

Porous materials exhibit significant moisture sorption curve hysteresis (Fig. 5). Capillary pressures keep a significant amount of water inside pores throughout consecutive wetting and drying operations. Several models have been developed in the literature to calculate intermediate variations in water content between the major adsorption—desorption curves in order to incorporate this feature in heat and mass transfer calculations (Hamdaoui et al. [22]).

Until recently, no simulation program has integrated hysteresis effects in its computational methods. When calculating the heat and moisture equations, any stated hysteresis model must be solved simultaneously. Therefore, a coupling with another software is mandatory and generally very complicated, requiring advanced programming skill. Also, this method is very computing time demanding.

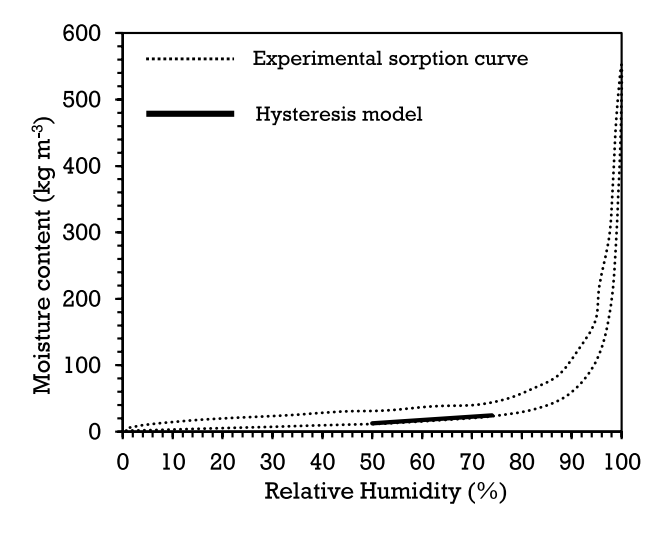
We propose to ease the simulation parameterization by simplifying the curve sorption while taking into account the hysteresis phenomenon. Based on previous studies on the effect of hysteresis on different materials construction, one can notice that, for type II sorption curves materials and whatever their adsorption/desorption potential capacity, the same material's behavior is observed: after several wetting—drying cycles (and for RH in the 30%—80% range, the sorption curve tends to become linear (Fig. 12). This part is described in detail in the following section.

Sorption linearization due to hysteresis effect

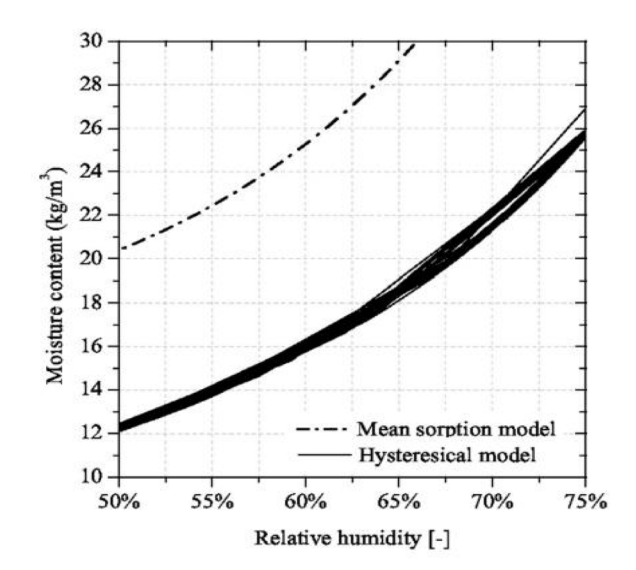
Several sorption hysteresis models are used (Hamdaoui et al. [22]), for physico-chemically interacting particles in small volumes and other phenomena like the ink-bottle pore effect. These models have shown their efficiency in improving the outputs of numerical results. However, their main disadvantages lie in both computation times and linkage to specific configurations and scenario.

The application of conceptual hysteresis models frequently results in a hysteretic behavior known as "pumping effect". It represents the fact that the quantitative scanning sorption curves do not follow the closure fundamental idea. In other words, there is a distinct water content value for each extreme of relative humidity during a series of adsorption and desorption cycles. As a result, a material that has been wetted and dried multiple times should generally recover to its original humidity levels and water content.

Promis et al. [26] used the Comsol Multiphysics software to analyze experimentally and computationally the hygrothermal response of hemp and rape straw concretes, taking into consideration the hysteresis phenomena. The authors demonstrated the evolution of water content as a function of RH in rape straw concretes, using a hysteresis model built



(a) Sorption curves of Promis et al. (Recopied from original)



(b) Sorption curves of Promis et al. (Original)

Fig. 12 Water vapor sorption hysteresis phenomena behavior of Promis et al. [26]



upon the measured material's adsorption curve (Fig. 12). For a relative humidity range of 50%–75%, the moisture hysteresis is practically on the adsorption curve and takes on a linear character with more cycles. We conclude based on the study of Promis et al. [26] that in the medium humidity range, hysteresis appears to have a minor impact on hydric behavior for relative humidity less than 80% and more than 50% in this instance (Fig. 12a). The use of a linear adsorption curve can yield satisfactory results.

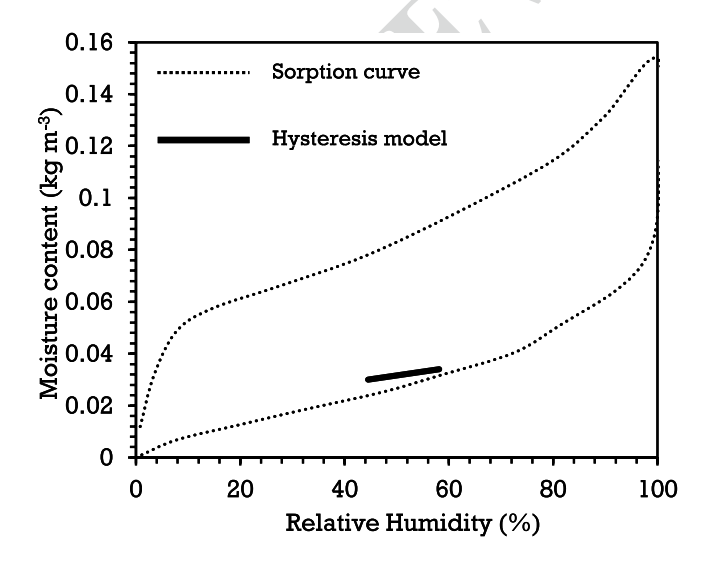
For similar materials Lelievre et al. [27] analyzed heat and moisture transport numerically by accounting for hysteresis and phase change effects. The authors demonstrate that Mualem's model appears to be more suited than Pedersen's to replicate sorption–desorption cycles (Fig. 13b). Hence, their sorption curve takes on a linear appearance after numerous cycles of adsorption/desorption for a humidity margin included between 40 and 60%, as illustrated in Fig. 13a.

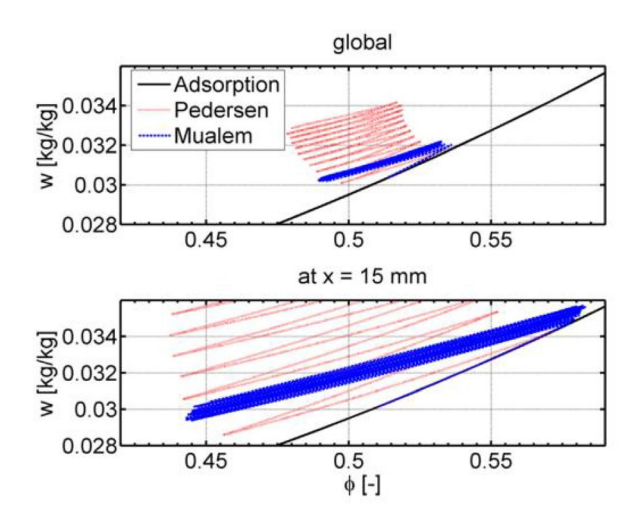
Maaroufi et al., [53] on the other hand, worked on demonstrating the effect of the sorption hysteresis phenomena on heat and moisture transport in an expanded polystyrene concrete (Fig. 14a). They developed a coupled heat and mass transport model that takes into consideration the sorption hysteresis phenomena. Their numerical outputs with and without the hysteresis phenomena were highlighted and compared to experiment data, demonstrating that taking the hysteresis phenomenon into account provides for a better understanding of the hygrothermal behavior of construction materials. In comparison to other studies, their hysteresis model was tested on a wide margin of relative humidity that reaches a high percentage close to 95%, where hygroscopic

medium will undergo saturation in terms of water content, and which explains why the average line of the adsorption/desorption curves is located almost in the center and not close to the main adsorption curve. Although the most relevant is that with a large number of humidification and dehumidification cycles the sorption curve tends to take a linear variation (Fig. 14b).

A simplified hysteresis model is proposed by Rémond et al. [54], suggesting a unique formulation to assess moisture sorption hysteresis in lignocellulosic materials by introducing the concept of a gripped box. Their model simply requires two modifiable parameters to be matched to the experimental data. The curves of a straight line through the mean sorption curve can describe the hysteresis phenomena between a defined interval of relative humidity and can be shifted according to the current state. One point is defined on the adsorption curve and the other one on the desorption curve passing by the mean sorption curve. This approach is limited if we have a plenty of wetting/drying cycle for a small relative humidity marge less than 20%, situated between 30 and 80% of relative humidity. Where the reverse point from desorption toward the adsorption cycle can be situated much below the desorption curve which demonstrated and validated in many studies [55, 56]. Their model needs to be coupled in existing computational software that can result in an increased computation time depending on the coupling method.

We suggest in this paper a method for linearizing the hysteresis cycles based on previous research works using the two points at 80% and 30% of relative humidity for the first adsorption curve.





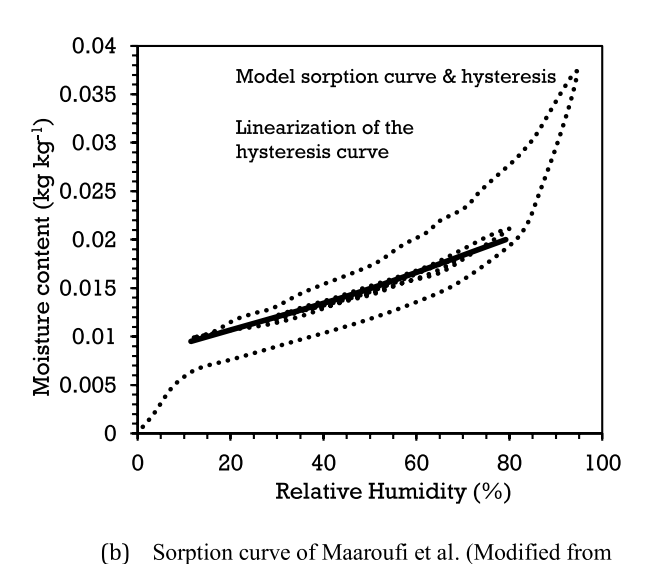
(a) Sorption curves of Lelievre et al (Recopied from original)

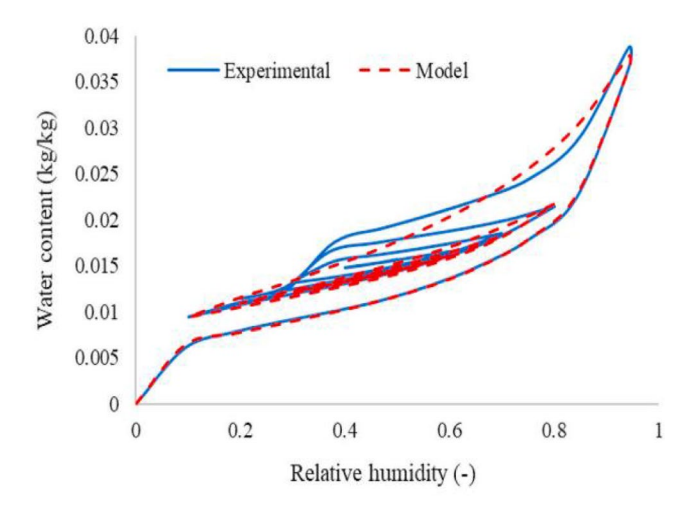
(b) Hysterisis effect

Fig. 13 Water vapor sorption hysteresis phenomena behavior of Lelievre et al. [27]



	Journal : Large 43452	Article No : 579	Pages : 26	MS Code : 579	Dispatch : 24-12-2022	1
--	-----------------------	------------------	------------	---------------	-----------------------	---





(a) Sorption curve

Fig. 14 Water vapor sorption hysteresis phenomena behavior of Maaroufi et al. [53]

original)

The first point of the linearized curve at 80% RH is on the first adsorption curve (Annex 1), generally, the RH inside the material in practical situation is far from being saturated with water content. It is assumed that the first hysteresis cycle starts with adsorption and then proceeds to desorption. For the second point of the linearized curve at 30% RH, the point takes on the value of water content at this humidity value by adding a ΔW % of difference between the first adsorption and desorption curves at 30% (12% for Mualem model and 10% for Promis model).

We validated our approach on Alioua et al. [21] data, at various depths (3, 7.5 and 12.5 cm). For this purpose, the linearized sorption curve of Alioua et al. [21] is obtained according to the following method where the first point located at 80% and the second at 30% RH, by adding a ΔW equal to 15%. The choice of the 15% value was made after a sensitivity study from 10 to 20%. The value of 15% represent the best configuration. The results found for this approach after linearization are compared with the results found by Alioua et al. [21] (with and without hysteresis effect) in the following section. The hygrothermal properties of Date Palm Concrete (DPC) are presented in the Table 11.

The linearized mathematical equation is written as below to determine the water content of the material based on the fitted sorption curve with GAB model:

$$\begin{split} W_{lin}(\phi) &= \left[2 \, GAB_{ads}(80\%) - \frac{17}{10} \, GAB_{ads}(30\%) - \frac{3}{10} \, GAB_{des}(30\%) \right] (\phi) \\ &+ \left[\frac{68}{50} \, GAB_{ads}(30\%) + \frac{12}{50} \, GAB_{des}(30\%) - \frac{3}{5} \, GAB_{ads}(80\%) \right] \end{split} \tag{8}$$

where Φ is the relative humidity situated between 0.3 and 0.8, GAB_{ads} is the first main adsorption curve fitted with

GAB model and GAB_{des} is the first main desorption curve fitted with the GAB model also.

Figure 15 represents the methodology of the work conducted on the experimental part to investigate the mechanical and hygrothermal properties of bio-based material. Numerical analysis was initiated to study the energy performance of the material by simplifying the modeling and taking into account the influence of hysteresis under challenging climate conditions.

4.2.3 Model validation of linearization effect on sorption curve with experimental data

Among the first researchers, Mendes et al. [60] are one of those who incorporated a linearization approach to simplify a difficult physical phenomena and accelerate the computation of hygrothermal behavior. The authors linearized the vapor exchange between the wall and the ambient air. This approach reduces the amount of time it takes to calculate the desired numerical outputs. In our case, we have worked on the linearization of the sorption curve based on the impact of the hysteresis effect for frequent adsorption and desorption cycles. The sorption curve has been linearized based on the following of multiple wetting and drying operations for a specified interval of relative humidity which must be situated between 30 and 80%.

We considered the linearization also, for a sorption curve of type II-isotherm [47] and for a material porosity situated between 0.3 and 0.9. Thus, the dynamics of heat and moisture transmission in DPC (Date Palm Concrete) [21], CLC (Coffee lightened Clay), and SC (Structural Cob) have been investigated. During the experiments, temperature (T) and



Table 11 Hygrothermal properties of Date Palm Concrete (DPC) (Taken from Alioua et al. study [21])

Property	Value	References	Property	Value	References
Dry density (kg m ⁻³)	954	[57]	Dry specific heat (J kg ⁻¹ K ⁻¹)	1500	[58]
Dry thermal conductivity $(W m^{-1} K^{-1})$	0.185	[57]	Moisture supplement of thermal conductivity (–)	10.190	[57]
Vapor resistance factor (dry cup) [-]	6.310	[59]	Vapor resistance factor (-)	5.570	[58]
Water sorption coefficient [kg m ⁻² s ^{-1/2}]	0.165	[57]	Water content at free saturation (kg m ⁻³)	429	[57]

relative humidity (RH) distributions across the wall thickness, as well as air parameters (T&RH) at the inside/outside environment, were continually recorded.

• Scenario 1. Temperature variation with constant humidity

Using the temperature profile of Scenario 1 (Fig. 10a), importing temperature and relative humidity values at

boundaries (from the experiments [21, 59] and taking initial conditions ($T=23\,^{\circ}\text{C}$ and RH=50%), we could simulate (Fig. 16) the temperature fluctuations at depths from 3 to 12.5 cm within the wall. The temperature profiles are better reproduced when accounting for linearized hysteresis than without, specifically for larger depths. However, in our case, the maximum differences between numerical and experimental results are obtained at 3 cm of depth and are equal to 2 $^{\circ}\text{C}$ and 2.8 $^{\circ}\text{C}$ for the larger and lower temperatures,

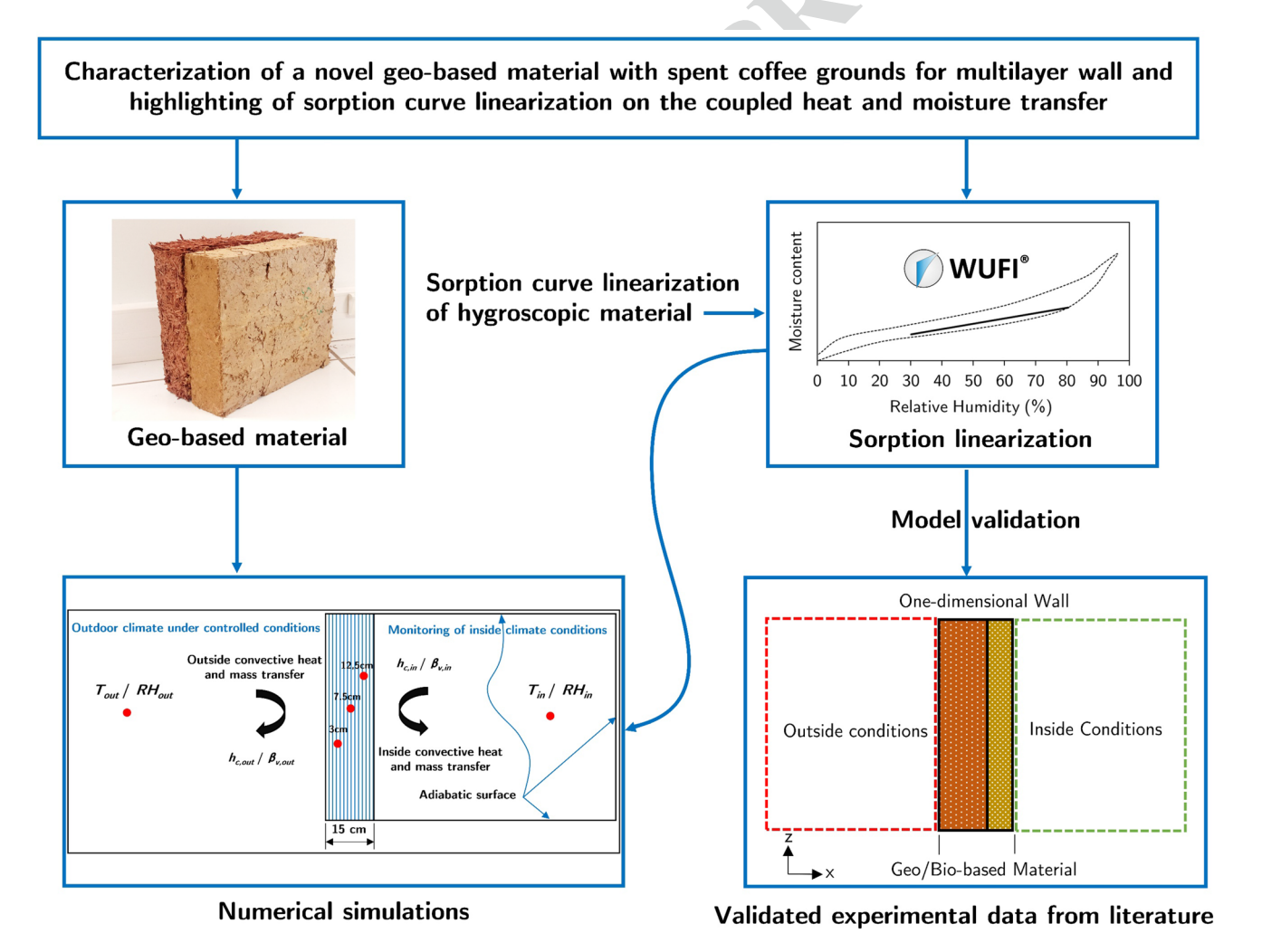


Fig. 15 Conceptual study plan



Journal: Large 43452	Article No : 579	Pages : 26	MS Code : 579	Dispatch : 24-12-2022	

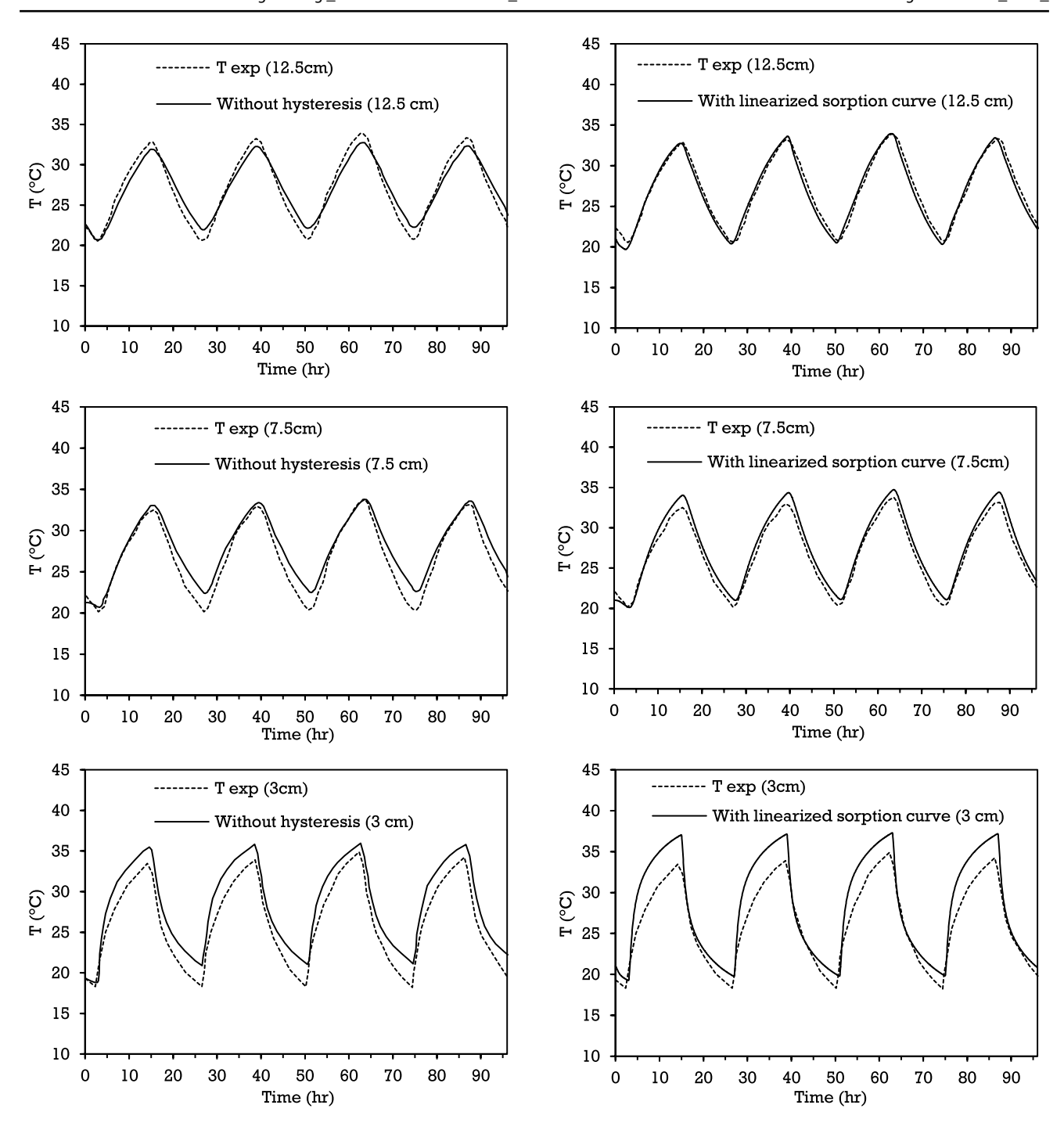


Fig. 16 Numerical and experimental temperature variations at various depths within the DPC wall by taken into account the linearisation of hysteresis effect

respectively. The root mean square error RMSE (Table 12) also are in favor of the linearization model concerning temperature estimates, even at 3 cm depth, though to a mess extent. The linearization for the two larger depths reduced the errors almost by half.

978

979

980

981

Table 12 Model comparison and validation for scenario 1

Depth (cm)	RMSE "Without hysteresis"	RMSE "With linearized sorption curve"
12.5	1.024	0.575
7.5	1.409	0.862
3.0	2.076	2.042



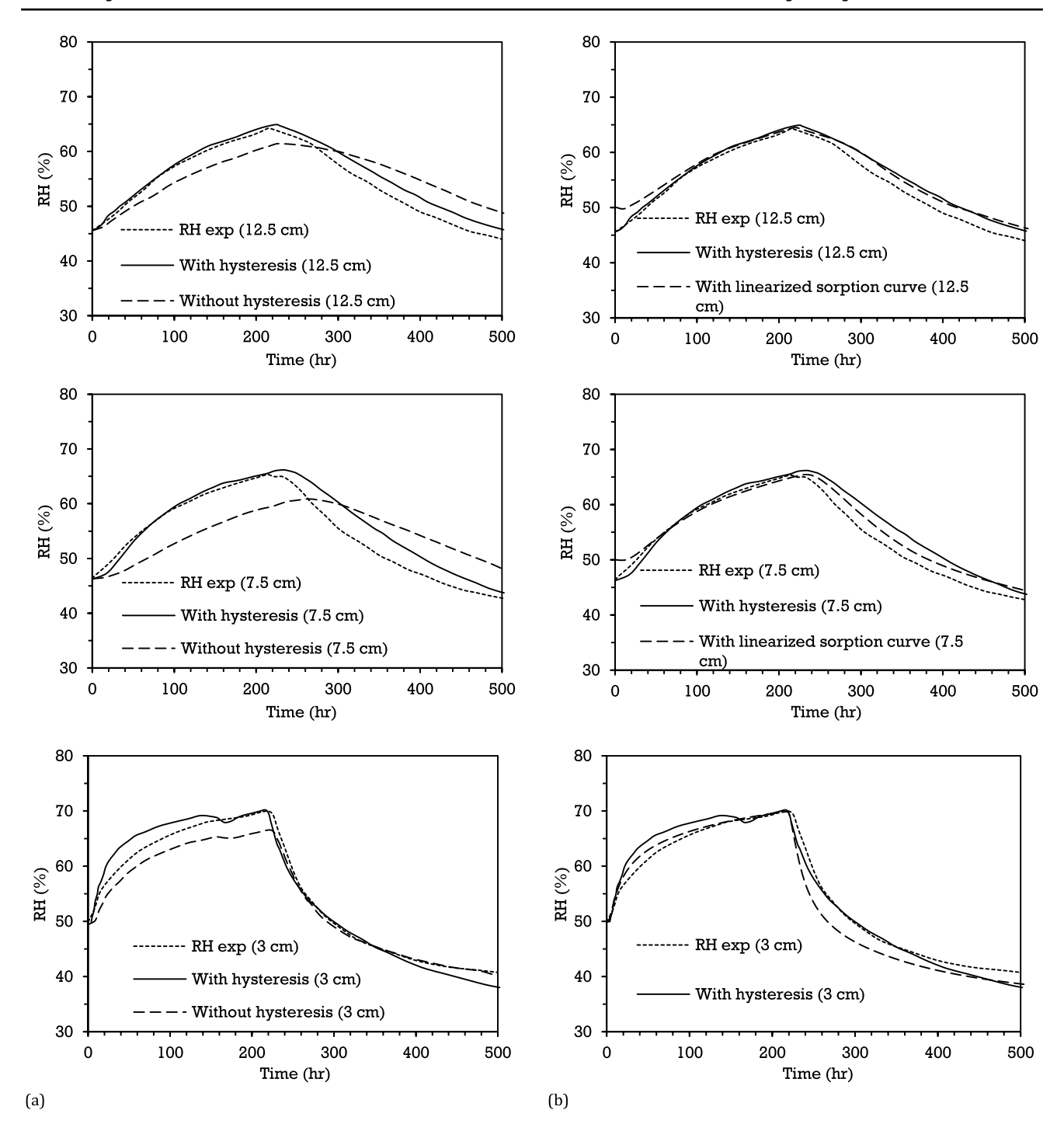


Fig. 17 Numerical and experimental humidity variations at various depths within the DPC wall by taken into account the linearization of hysteresis effect

Scenario 2. Humidity variation with isotherm condition

With the RH profile of Scenario 2 (Figure 10b), simulations without hysteresis effect are always underestimating water uptaking during the adsorption curve (Figure 17), compared to experimental data. At desorption, the curves

Table 13 Model comparison and validation for scenario 2

Depth (cm)	RMSE "With- out hysteresis"	RMSE "With hysteresis"	RMSE "With linearized sorption curve"
12.5	3.535	1.572	1.564
7.5	5.586	2.389	1.529
3.0	2.025	2.008	2.325



983

984

985

986

987

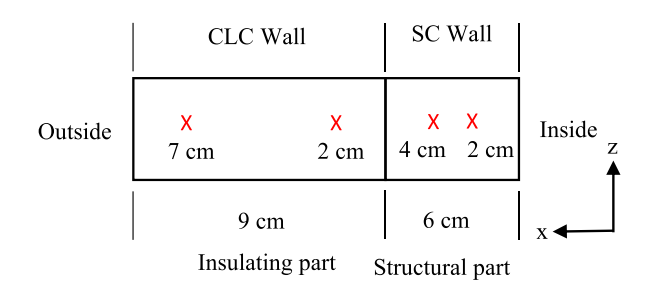


Fig. 18 Schematics of the multilayer wall composed of SC+CLC and the measured points

without hysteresis (Figure 17a) maintain too much water inside the wall compared to measurements. When the linearization approximation of the sorption curve is included in the simulations, the simulated RH profiles improve significantly at intermediate depths. For the largest depth of

12.5 cm, linearization slightly overestimates water uptake during adsorption, then does not significantly deviate from the usual hysteresis simulation at desorption. At the smallest depth, linearization tends to decrease water uptake, which favors a better RH simulation during adsorption, but a rather high-water desorption compared to experiments and usual hysteresis simulation. These tendencies are reflected in the overall RMSE values (Table 13) with a largest difference between experience and simulations for the two largest depths, while at 3 cm wall depth, as depicted by Alioua et al [21], the hysteresis effect does not have a significant effect on the accuracy, an also valid observation with our linearization approach.

4.2.4 Hygrothermal performance evaluation of CLC and SC wall

WUFI Plus' simulations were applied to a double wall structure (Fig. 18) composed of the SC and CLC components

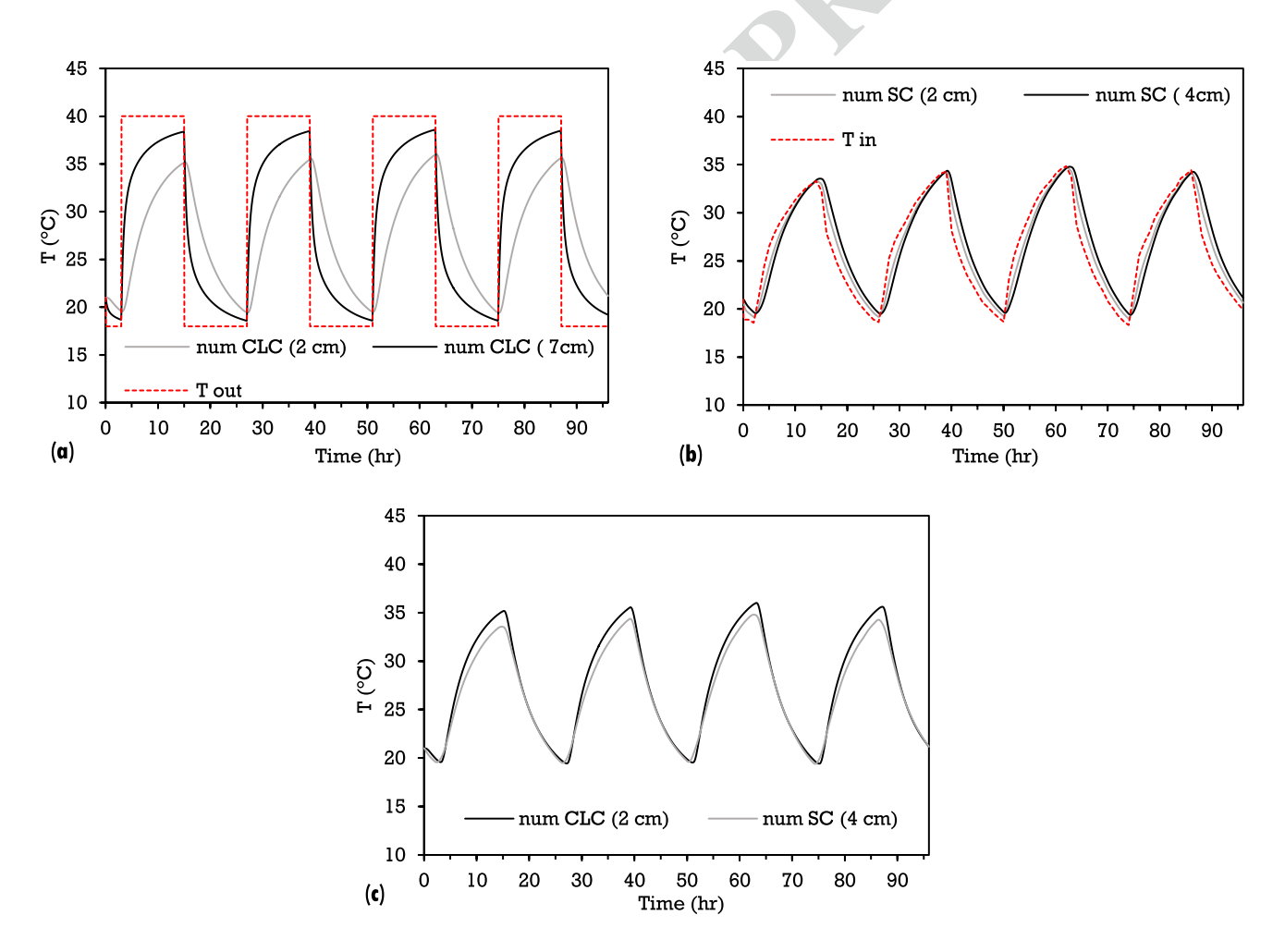
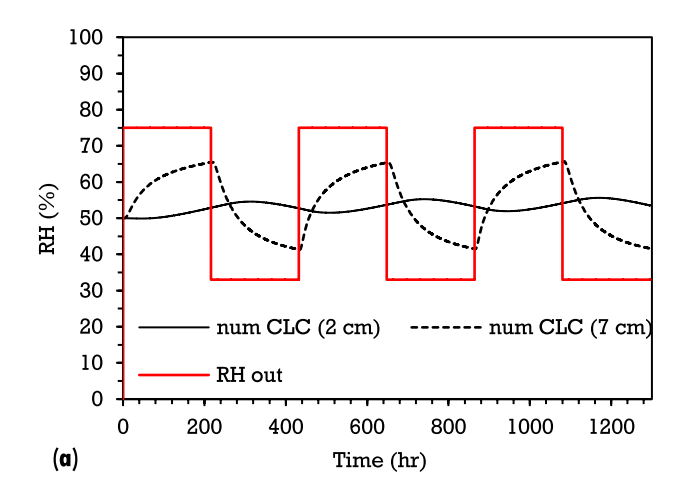


Fig. 19 Numerical investigation of temperature variations at various depths within the SC+CLC multilayered wall by considered the linearization of hysteresis effect





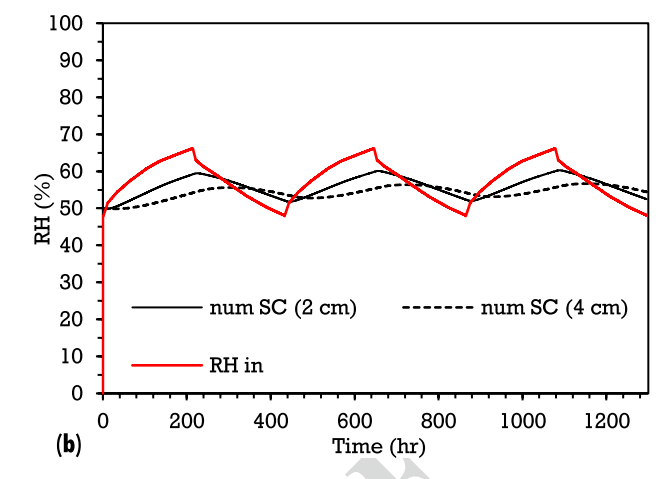


Fig. 20 Numerical investigation of humidity variations at various depths within the SC+CLC multilayered wall using linearization of the RH hysteresis cycle

previously described, with corresponding sorption isotherms, vapor resistance factors, thermal conductivity and heat capacity (Figs. 2, 3 and 4).

• Scenario 1. Temperature variation with constant humidity

Thermal behavior of the SC and CLC components of the wall are different especially at the wall's surfaces. For the CLC component (Fig. 19a), a remarkable drop in amplitude is observed between the two wall boundaries where we can see an amplitude delay in the thermal behavior of the wall caused by the rapid transition in outside temperature. After 12 h, the CLC at 7 cm closer to the outside environment undergoes a strong evolution of temperature that reaches 38.5 °C, while only 34 °C is reached deeper in the wall, at 2 cm (Fig. 19a).

A slight maximum temperature difference exists (Fig. 19c), between the 2 cm CLC and 4 cm SC measured points, because of their relative distance. Also, while the internal surface is exposed to the variable temperature. The temperature decreases again at 2 cm for the SC wall and reaches 32.9 °C (Fig. 19b), compared to the 7 cm of CLC wall, which makes us gain a decrease of 5.6 °C compared to the external temperature value.

Scenario 2. Humidity variation with isotherm condition

In this scenario, the inside temperature is kept constant (23 °C) while the outside wall subjected to RH variations. The outside wall is exposed to 216 h long RH plateaus of 75% and 33% successively. Simulated relative humidity evolutions inside the walls at the four depths. (Fig. 20b) show a lower amplitude of variations closer to the inside in the

SC wall. Furthermore, a remarkable delay of response is observed between 2 and 4 cm depths SC, as a sign for a larger impermeability of the structural wall.

After 216 h, the SC at 2 cm absorbs the maximum amount of moisture (60%), while at 4 cm, material continues to absorb moisture, which explains why the two depths do not have the same sorption. This phenomenon has not been noted for DCP [59]. Furthermore, during the desorption phase, the RH decreases more rapidly at 4 cm, compared to the 2 cm.

A similar trend is observed for the CLC (Fig. 20a), a delay of response is observed between 2 and 7 cm for RH wave fronts, however less pronounced than in the SC wall since CLC exhibits a larger water permeability. During the sorption phase, the relative humidity increases more rapidly with a maximum of 65% at the location near the outside of the wall, compared to the other location deeper in the wall. As for SC, the CLC wall does not have the same absorption

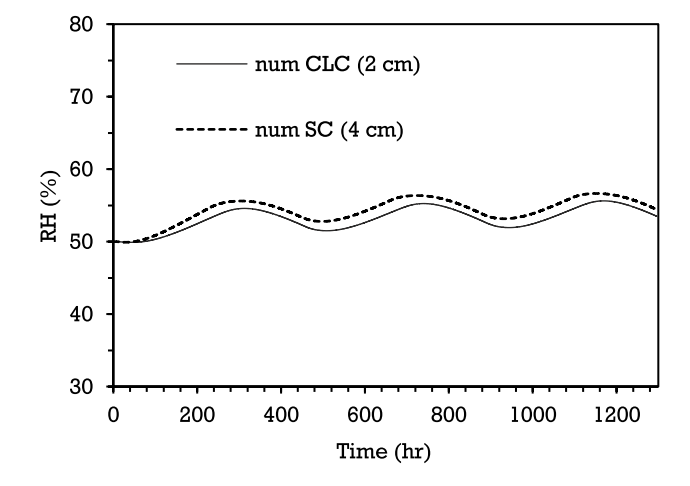


Fig. 21 Moisture behavior of the interface between CLC and SC walls



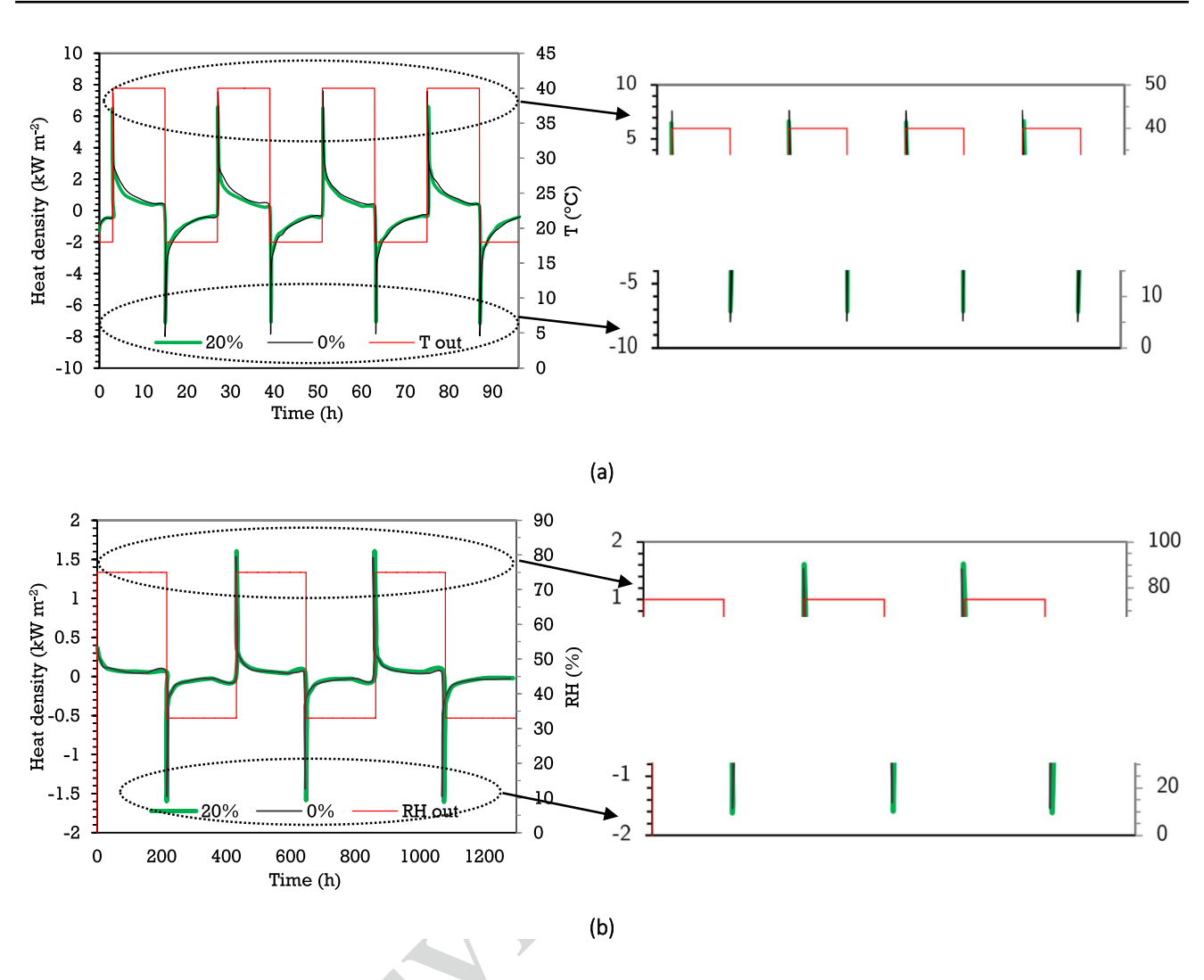


Fig. 22 Quantitative analysis of the energy performance of multilayered wall (SC+CLC) for isotherm (a) and isohydric (b) scenarios

and desorption process for the two depths. The junction between CLC and SC is influenced by both indoor and outdoor humidity variations. Figure 21 shows that, unlike the results in Fig. 20 that the RH variations for the two 4 cm (SC) and 2 cm (CLC) positions are exhibiting close hygroscopic behaviors, with a slight difference in humidity between the two positions only due to their closely locations in the double wall structure.

Heat flow transfer through the CLC + SC wall for isotherm and isohydric scenario

Hygrothermal transfer generates a flow density which is usually not quantified. For this purpose, Fig. 22 shows the heat flux density generated for the SC+CLC wall for 0% and 20% of coffee ground wastes in the insulating CLC component. Considering the variations of temperature (Fig. 22a) and humidity (Fig. 22b), these simulations show that the

CLC+SC wall with CGW, allows less heat to pass than without the inclusion of CGW in the material due to the high gradient in temperature and humidity. This difference for the case of Fig. 22a, is due to the decrease in thermal conductivity of the wall by the coffee ground wastes. A different trend is observed on the Fig. 22b, where the heat flux density gain increases basically (with CGW included) due to the porosity increased by coffee ground wastes (see Fig. 3b). Thus, the wall captures more moisture upon CGW addition, due to the phase change enthalpy of water, this will be added as a form of energy for the wall.

Simulation results reproduce dynamic variations of the heat flux through the SC+CLC wall façade for isotherm and isohydric scenario. In the Fig. 22a, we kept the relative humidity constant at 50% and the temperature was varied between 18 and 40°c. We observed two phases: (i) the heat peak phase related to the temperature peak and (ii) the heat release phase when the temperature drops. In the first phase, we see that the



1095

1096

1097

1098

1099

1100

1101

1102

1103

1104

1105

1106

1107

1108

1109

1110

1111

1112

1114

1115

1116

1117

1118

1119

1120

1121

1122

1123

1124

1125

1126

1127

1128

1129

1130

1131

1132

1133

1134

1135

1136

1137

1138

1139

1140

1141

1142

1143

1144

1145

1146

1147

1148

1149

1150

1151

1152

1153

1154

1155

1156

1157

1158

1159

1160

1161

1162

1163

1164

1165

1166

1167

peak is higher in the case of CLC wall with 0% coffee ground wastes (7.48 kW m⁻²) than in the case with 20% coffee ground wastes (6.62 kW m⁻²). On the other hand, the opposite effect is observed when the temperature drops. The wall with 20% coffee ground wastes releases less heat than the wall with 0% coffee grounds. The ability to store and release heat is related to the improvement of the heat capacity and thermal conductivity of the wall by CGW. This difference generates a dynamic variation of 12% in the quantity of heat passing through the wall over a well-defined time interval (at time 3 h).

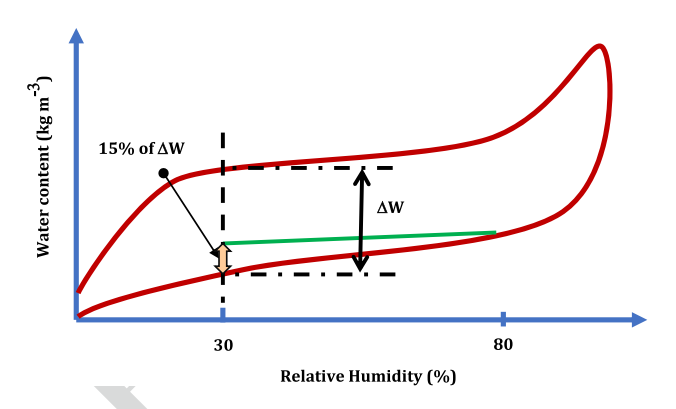
For the second investigation (Fig. 22b), we applied an isotherm scenario where we keep a constant temperature of air on both sides, at 23 °C, and variating only the relative humidity between 33 and 75% for several cycles to better understand the energy behavior in term of moisture residues. This last one gives us the possibility to know the heat flow transmitted through a wall when imposing a moisture gradient between two surfaces and also to know the effect of the difference of porosity on the heat flow transmitted. As shown in the Fig. 22b. we find that for a dynamic change in relative humidity, the heat flux density registers a peak of 1.61 kW m⁻² and 1.53 kW m⁻², respectively, for a percentage of 20% and 0% of coffee ground wastes in the CLC wall formulation. This heat peak is explained by the difference in the internal structure in terms of material porosity. For the CLC wall with 0% and 20% of coffee ground wastes, we observe on Fig. 3b that the porosity varies from 0.46 to 0.63 which represents an increase of 37%. This difference generates a dynamic variation of 8% of the amount of heat density flux that passes through the wall over a defined time range. We conclude that addition of CGW increases the porosity which facilitates the absorption/desorption cycle and lets more heat pass through due to the enthalpy of phase change.

5 Conclusion

The mechanical and hygrothermal assessment of cob walls incorporating CGW at various concentration levels was the focus of this research. The addition of up to 20% CGW to the insulating cob matrix increases the material's performance, both in terms of heat storage capacity, thermal insulation and compressive strength. When compared to conventional cob building materials, the compressive strength and hygrothermal performance of CLC material containing CGW results in a reduction of the cob wall thickness. The widespread valorization of CGW could significantly contribute to the achievement of sustainable development goals, provided such spares do not get a better use elsewhere.

We analyzed numerically the effect of sorption isotherm linearization on the hygrothermal behavior of a hygroscopic wall built of low-carbon material and validated the approach experimentally. Hysteresis linearization can help thermal engineers to achieve more accurate building performance analyses in a fast and efficient way. The suggested approach has a decent accuracy for various depths for both heat and mass transfers. When the linearization of the hysteretic sorption curve is included in the simulations, the accuracy improves significantly.

Appendix



Annex 1 Moisture sorption isotherm linearized of Date Palm Concrete (DPC) [21] (Refitted and modified from original)

Acknowledgements This research is associated with the French DD&RS strategy (Sustainable Development and Social Responsibility).

Author contributions Conceptualization: M-AH, M-HB, YE; Methodology: M-AH, M-HB, YE; Formal analysis and investigation: M-AH, M-HB, YE, DC, SG; Writing—original draft preparation: M-AH, M-HB, YE; Writing—review and editing: M-AH, M-HB, YE, DC; Supervision: M-HB, DC, YE.

Funding No funding.

Data availability Data are available. Author declared that all data and materials as well as software application support his published claims and comply with field standards.

Declarations

Conflict of interest The authors have no relevant financial or non-financial interests to disclose.

Ethical approval Not applicable.

Research involving human participants and/or animals Not applicable.

Consent for publication All authors agree to publish.

 $\underline{\underline{\mathscr{D}}}$ Springer

1232

1233

1234

1235

1236

1237

1238

1239

1240

1241

1242

1243

1244

1245

1246

1247

1248

1249

1250

1251

1252

1253

1254

1255

1256

1257

1258

1259

1260

1261

1262

1263

1264

1265

1266

1267

1268

1269

1270

1271

1272

1273

1274

1275

1276

1277

1278

1279

1280

1281

1282

1283

1284

1285

1286

1287

1288

1289

1290

1291

1292

1293

1294

1295

1296

1168 References

1172

1173

1174

1175

1176

1177

1178

1179

1180

1181

1182

1183

1184

1185

1186

1187

1188

1189

1190

1191

1192

1193

1194

1195

1196

1197

1198

1199

1200

1201

1202

1203

1204

1205

1206

1207

1208

1209

1210

1211

1222

1223

1224

1225

- Esfanjary Kenari E. Persian historic urban landscapes interpreting and managing Maibud over 6000 years. Edinburgh University Press; 2017.
 - Bouasria M, El Mendili Y, Benzaama M-H, Pralong V, Bardeau J-F, Hennequart F. Valorisation of stranded laminaria digitata seaweed as an insulating earth material. Constr Build Mater. 2021;308: 125068. https://doi.org/10.1016/j.conbuildmat.2021. 125068.
 - Riffat MASB. Building energy consumption and carbon dioxide emissions: threat to climate change. J Earth Sci Clim Change. 2015. https://doi.org/10.4172/2157-7617.S3-001.
 - Lekshmi MS, Vishnudas S, Nair DG. An investigation on the potential of mud as sustainable building material in the context of Kerala. Int J Energy Technol Policy. 2017;13(1-2):107-22. https://doi.org/10.1504/IJETP.2017.080621.
 - El Mendili Y, et al. Mud-based construction material: promising properties of French gravel wash mud mixed with byproducts, seashells and fly ash as a binder. Materials. 2021;14(20):20. https:// doi.org/10.3390/ma14206216.
 - Miccoli L, Müller U, Fontana P. Mechanical behaviour of earthen materials: a comparison between earth block masonry, rammed earth and cob. Constr Build Mater. 2014;61:327–39. https://doi. org/10.1016/j.conbuildmat.2014.03.009.
 - Bekhiti M, Trouzine H, Rabehi M. Influence of waste tire rubber fibers on swelling behavior, unconfined compressive strength and ductility of cement stabilized bentonite clay soil. Constr Build Mater. 2019;208:304–13. https://doi.org/10.1016/j.conbuildmat. 2019.03.011.
 - Chang I, et al. Review on biopolymer-based soil treatment (BPST) technology in geotechnical engineering practices. Transp Geotech. 2020;24: 100385. https://doi.org/10.1016/j.trgeo.2020.100385.
 - Chang I, Im J, Cho G-C. Introduction of microbial biopolymers in soil treatment for future environmentally-friendly and sustainable geotechnical engineering. Sustainability. 2016;8(3):3. https://doi. org/10.3390/su8030251.
 - Ben-Hur M, Malik M, Letey J, Mingelgrin U. Adsorption of polymers on clays as affected by clay charge and structure, polymer properties, and water quality. Soil Sci. 1992. https://doi.org/10.1097/00010694-199205000-00002.
 - Vásquez-Garay F, Carrillo-Varela I, Vidal C, Reyes-Contreras P, Faccini M, Teixeira Mendonça R. A review on the lignin biopolymer and its integration in the elaboration of sustainable materials. Sustainability. 2021;13(5):5. https://doi.org/10.3390/su13052697.
- 12.1 Cerino-Córdova FJ, Dávila-Guzmán NE, García León AM,
 12.1 Salazar-Rabago JJ, Soto-Regalado E. Revalorization of coffee
 12.1 waste. In: Toledo Castanheira D, editor. Coffee production and
 12.1 research. IntechOpen; 2020. p. 5–10.
- 1216 13. Levy D, Reinecke J, Manning S. The political dynamics of sustainable coffee: contested value regimes and the transformation of sustainability. J Manag Stud. 2016;53(3):364–401. https://doi. 1219 org/10.1111/joms.12144.
- 1220 14. International Coffee Organization What's New. https://www.ico.
 1221 org/. Accessed 13 Feb 2022
 - Mata TM, Martins AA, Caetano NS. Bio-refinery approach for spent coffee grounds valorization. Bioresour Technol. 2018;247:1077–84. https://doi.org/10.1016/j.biortech.2017.09. 106.
- 1226 16. Pujol D, et al. The chemical composition of exhausted coffee waste. Ind Crops Prod. 2013;50:423–9. https://doi.org/10.1016/j. indcrop.2013.07.056.
- 1229 17. Mussatto SI, Machado EMS, Martins S, Teixeira JA. Production, composition, and application of coffee and its industrial residues.

- Food Bioprocess Technol. 2011;4(5):661. https://doi.org/10.1007/s11947-011-0565-z.
- Abahri K, Belarbi R, Oudjehani N, Issaadi N, Ferroukhi M. Total pressure gradient incidence on hygrothermal transfer in highly porous building materials. Adv Mater Res. 2013;772:124–9. https://doi.org/10.4028/www.scientific.net/AMR.772.124.
- Ferroukhi MY, Djedjig R, Limam K, Belarbi R. Hygrothermal behavior modeling of the hygroscopic envelopes of buildings: a dynamic co-simulation approach. Build Simul. 2016;9(5):501–12. https://doi.org/10.1007/s12273-016-0292-5.
- Slimani Z, Trabelsi A, Virgone J, Zanetti Freire R. Study of the hygrothermal behavior of wood fiber insulation subjected to nonisothermal loading. Appl Sci. 2019;9(11):11. https://doi.org/10. 3390/app9112359.
- Alioua T, Agoudjil B, Chennouf N, Boudenne A, Benzarti K. Investigation on heat and moisture transfer in bio-based building wall with consideration of the hysteresis effect. Build Environ. 2019;163: 106333. https://doi.org/10.1016/j.buildenv.2019. 106333.
- Hamdaoui M-A, Benzaama M-H, El Mendili Y, Chateigner D. A review on physical and data-driven modeling of buildings hygrothermal behavior: models, approaches and simulation tools. Energy Build. 2021;251: 111343. https://doi.org/10.1016/j.enbuild.2021.111343.
- Zhang Z, Thiery M, Baroghel-Bouny V. A review and statistical study of existing hysteresis models for cementitious materials. Cem Concr Res. 2014;57:44. https://doi.org/10.1016/j.cemconres. 2013.12.008.
- 24. Mualem Y. Modified approach to capillary hysteresis based on a similarity hypothesis. Water Resour Res. 1973;9(5):1324–31. https://doi.org/10.1029/WR009i005p01324.
- 25. Mualem Y. A conceptual model of hysteresis. Water Resour Res. 1974;10(3):3. https://doi.org/10.1029/WR010i003p00514.
- Promis G, Douzane O, Le Tran AD, Langlet T. Moisture hysteresis influence on mass transfer through bio-based building materials in dynamic state. Energy Build. 2018;166:450–9. https://doi.org/ 10.1016/j.enbuild.2018.01.067.
- Lelievre D, Colinart T, Glouannec P. Hygrothermal behavior of bio-based building materials including hysteresis effects: experimental and numerical analyses. Energy Build. 2014;84:617–27. https://doi.org/10.1016/j.enbuild.2014.09.013.
- Zhang X, Chen B, Riaz Ahmad M. Characterization of a novel bio-insulation material for multilayer wall and research on hysteresis effect. Constr Build Mater. 2021;290:123162. https://doi. org/10.1016/j.conbuildmat.2021.123162.
- Patera A, Derluyn H, Derome D, Carmeliet J. Influence of sorption hysteresis on moisture transport in wood. Wood Sci Technol. 2016;50(2):259–83. https://doi.org/10.1007/s00226-015-0786-9.
- 30. Volhard F. Light earth building: a handbook for building with wood and earth. Walter de Gruyter GmbH; 2016.
- Sluiter A, Hames B, Ruiz RO, Scarlata C, Sluiter J, Templeton D. Determination of structural carbohydrates and lignin in biomass. Biomass Anal Technol Team Lab Anal Proced. 2004;2011:1–14.
- Mussatto SI, Ballesteros LF, Martins S, Teixeira JA. Extraction of antioxidant phenolic compounds from spent coffee grounds. Sep Purif Technol. 2011;83:173–9. https://doi.org/10.1016/j.seppur. 2011.09.036.
- Grembecka M, Malinowska E, Szefer P. Differentiation of market coffee and its infusions in view of their mineral composition. Sci Total Environ. 2007;383:59–69. https://doi.org/10.1016/j.scitotenv.2007.04.031.
- Köbbing J, Thevs N, Zerbe S, Wichtmann W, Couwenberg J. The utilisation of reed (Phragmites australis): a review," undefined, 2013. [Online]. Available: https://www.semanticscholar.org/paper/The-utilisation-of-reed-(Phragmites-australis)%3A-a-K%C3%B6bbing-Thevs/307c5503de54c11cdbd325f1f28491b561cc75eb. Accessed 15 Feb 2022.



1298

1299

1300

1301

1302

1303

1304

1305

1306

1307

1308

1309

1310

1311

1312

1313

1314

1315

1316

1317

1318

1319

1320

1321

1322

1323

1324

1325

1326

1327

1328

1329

1330

1331

1332

1333

1334

1335

1336

1337

1338

1339

1340

1341

1342

1343

1344

1345

1346

1347

1348

1349

1350

1351

1352

- Gražulis S, et al. Crystallography open database (COD): an openaccess collection of crystal structures and platform for world-wide collaboration. Nucleic Acids Res. 2012;40:420–7. https://doi.org/ 10.1093/nar/gkr900.
- Lutterotti L, Matthies S, Wenk H-R, Schultz AS, Richardson JW. Combined texture and structure analysis of deformed limestone from time-of-flight neutron diffraction spectra. J Appl Phys. 1997;81(2):594–600. https://doi.org/10.1063/1.364220.
- 37. El Mendili Y, et al. Combined XRF, XRD, SEM-EDS, and Raman analyses on serpentinized harzburgite (Nickel Laterite Mine, New Caledonia): implications for exploration and geometallurgy. ACS Earth Space Chem. 2019;3:2237–49. https://doi.org/10.1021/acsearthspacechem.9b00014.
- 38. Meinhold G. Rutile and its applications in earth sciences. Earth-Sci Rev. 2010;102(1):1–28. https://doi.org/10.1016/j.earscirev. 2010.06.001.
- Stanienda KJ. Carbonate phases rich in magnesium in the Triassic limestones of the eastern part of the Germanic Basin. Carbonates Evaporites. 2016;31(4):387–405. https://doi.org/10.1007/s13146-016-0297-2.
- Andrade FA, Al-Qureshi HA, Hotza D. Measuring the plasticity of clays: a review. Appl Clay Sci. 2011;51(1):1–7. https://doi.org/ 10.1016/j.clay.2010.10.028.
- 41. Hillel D. Soil physical attributes. In: Hillel D, editor. Soil in the environment. San Diego: Academic Press; 2008. p. 55–77.
- 42. Miranda-Trevino JC, Coles CA. Kaolinite properties, structure and influence of metal retention on pH. Appl Clay Sci. 2003;23(1):133–9. https://doi.org/10.1016/S0169-1317(03) 00095-4.
- 43. NF EN ISO 12572. Afnor EDITIONS. https://www.boutique.afnor.org/fr-fr/norme/nf-en-iso-12572/performance-hygrothermique-des-materiaux-et-produits-pour-le-batiment-deter/fa184538/57928. Accessed 27 Jul 2022
- NF ISO 5017. Afnor EDITIONS. https://www.boutique.afnor. org/fr-fr/norme/nf-iso-5017/produits-refractaires-faconnesdenses-determination-de-la-masse-volumique-a/fa169530/41164. Accessed 27 Jul 2022
- NF EN ISO 11357-4. Afnor EDITIONS. https://www.boutique. afnor.org/fr-fr/norme/nf-en-iso-113574/plastiques-analyse-calor imetrique-differentielle-dsc-partie-4-determination/fa199556/ 238238. Accessed 27 Jul 2022
- NF EN ISO 12571. Afnor EDITIONS. https://m.boutique.afnor. org/fr-fr/norme/nf-en-iso-12571/performance-hygrothermiquedes-materiaux-et-produits-pour-le-batiment-deter/fa177734/ 42249. Accessed 27 Jul 2022
- Andrade R, Pérez C. Models of sorption isotherms for food: uses and limitations. Vitae Rev Fac Quimica Farm. 2011;18:325–34.
- 48. Moodley P, Trois C. Lignocellulosic biorefineries: the path forward. In: Ray RC, editor. Sustainable biofuels. Academic Press; 2021. p. 21–42.
- Glasser WG, Barnett CA, Sano Y. Classification of lignins with different genetic and industrial origins. J Appl Polym Sci Appl Polym Symp U. S. Art. no. CONF-8205234-Vol.1, Jan. 1983.
 [Online]. Available: https://www.osti.gov/biblio/7146700-class ification-lignins-different-genetic-industrial-origins. Accessed 27 Feb 2022

 Sena da Fonseca B, Vilão A, Galhano C, Simão JAR. Reusing coffee waste in manufacture of ceramics for construction. Adv Appl Ceram. 2014;113(3):159–66. https://doi.org/10.1179/17436 76113Y.0000000131.

1353

1354

1355

1356

1357

1358

1359

1360

1361

1362

1363

1364

1365

1366

1367

1368

1369

1370

1371

1372

1373

1374

1375

1376

1377

1378

1379

1380

1381

1382

1383

1384

1385

1386

1387

1388

1389

1390

1391

1392

1393

1394

1395

1396

1397

1398

1399

- Eliche-Quesada D, et al. The use of different forms of waste in the manufacture of ceramic bricks. Appl Clay Sci. 2011;52:270–6. https://doi.org/10.1016/j.clay.2011.03.003.
- Künzel HM. Simultaneous heat and moisture transport in building components: one- and two-dimensional calculation using simple parameters. Stuttgart: IRB-Verl; 1995.
- Maaroufi M. Experimental and numerical highlighting of water vapor sorption hysteresis in the coupled heat and moisture transfers. J Build Eng. 2021;40:102321.
- Rémond R, Almeida G, Perré P. The gripped-box model: a simple and robust formulation of sorption hysteresis for lignocellulosic materials. Constr Build Mater. 2018;170:716–24. https://doi.org/ 10.1016/j.conbuildmat.2018.02.116.
- Zhang Z. Modelling of sorption hysteresis and its effect on moisture transport within cementitious materials. p. 237.
- Huang H-C, Tan Y-C, Liu C-W, Chen C-H. A novel hysteresis model in unsaturated soil. Hydrol Process. 2005;19(8):1653–65. https://doi.org/10.1002/hyp.5594.
- Haba B, Agoudjil B, Boudenne A, Benzarti K. Hygric properties and thermal conductivity of a new insulation material for building based on date palm concrete. Constr Build Mater. 2017;154:963– 71. https://doi.org/10.1016/j.conbuildmat.2017.08.025.
- Benmansour N, Agoudjil B, Gherabli A, Kareche A, Boudenne A. Thermal and mechanical performance of natural mortar reinforced with date palm fibers for use as insulating materials in building. Energy Build. 2014;81:98–104. https://doi.org/10.1016/j.enbuild. 2014.05.032.
- Chennouf N, Agoudjil B, Alioua T, Boudenne A, Benzarti K. Experimental investigation on hygrothermal performance of a biobased wall made of cement mortar filled with date palm fibers. Energy Build. 2019;202: 109413. https://doi.org/10.1016/j.enbuild.2019.109413.
- Mendes N, Philippi PC, Lamberts R. A new mathematical method to solve highly coupled equations of heat and mass transfer in porous media. Int J Heat Mass Transf. 2002;45(3):509–18. https:// doi.org/10.1016/S0017-9310(01)00172-7.

Publisher's Note Springer Nature remains neutral with regard to jurisdictional claims in published maps and institutional affiliations.

Springer Nature or its licensor (e.g. a society or other partner) holds exclusive rights to this article under a publishing agreement with the author(s) or other rightsholder(s); author self-archiving of the accepted manuscript version of this article is solely governed by the terms of such publishing agreement and applicable law.